Journal of Radioanalytical and Nuclear Chemistry (2024) 333:4333–4352
https://doi.org/10.1007/s10967-024-09570-y

Gamma emission from interaction of fission neutrons on nickel and zirconium

Eric Mauerhofer[1] · Niklas Ophoven[1,4] · Zeljko Ilic[1,2] · Christian Stieghorst[3] · Zsolt Révay[3] · Iaroslav Meleshenkovskii[1] · Tsitohaina H. Randriamalala[1]

Received: 19 March 2024 / Accepted: 19 May 2024 / Published online: 11 June 2024

Abstract
Gamma emission induced by the irradiation of nickel and zirconium with fission neutrons was investigated with the FaNGaS (Fast Neutron–induced Gamma-ray Spectrometry) instrument operated at Heinz Maier-Leibnitz Zentrum. Measurements were done at an angle of 90° with respect to the direction of the fission neutron beam (average neutron energy of 2.18 MeV). We report on the relative intensities and production cross sections of 265 gamma lines (163 for nickel and 102 for zirconium). Consistency with available literature data was evaluated. The cross section of the ^{90}Zr(n,n′)^{90m}Zr reaction was determined to be 88 ± 8 mb. For a counting time of 12 h, the detection limits of 0.7 and 1.3 mg were estimated for nickel and zirconium, respectively.

Keywords Cross section · Detection limits · Fission neutrons · Inelastic scattering · Nickel · Zirconium

Introduction

The FaNGaS (Fast Neutron induced Gamma-ray Spectrometry) instrument [1–3] installed at Heinz Maier-Leibnitz Zentrum (MLZ) offers the possibility to perform non-destructive elemental analysis of samples of various sizes origins by means of Prompt Gamma Analysis based on Inelastic Neutron Scattering PGAINS as we are going to call the method from now on. This analytical technique focuses on the measurement of prompt gamma radiation emitted from inelastic scattering of fission neutrons, i.e. (n,n′γ) reactions. In some cases, prompt gamma rays induced by other reactions like (n,pγ), (n,αγ) or (n,γ) as well as delayed gamma rays of activation products formed by the aforementioned reactions can be detected as well. At MLZ, fission neutrons are generated from a uranium converter (93% of ^{235}U) plugged into the heavy water moderator of the research reactor FRM II (Forschungs-Neutronenquelle Heinz Maier-Leibnitz). An intense beam of fission neutrons with an average energy of 2.18 MeV is extracted from the beamtube SR10 (Strahlrohr 10) into the MEDAPP (Medical Application) irradiation room via a set of filters and collimators. A well-shielded electromechanically-cooled n-type HPGe-detector of 50% relative efficiency is used for the detection of the neutron-induced gamma rays. Gamma-ray spectra are recorded at an angle of 90° with respect to the axis of the incident neutron beam.

To perform a precise elemental analysis of samples by means of the PGAINS technique, reliable and accurate information on the fission-neutrons induced (n,n′γ) reactions, i.e. the gamma-ray energies and the gamma-ray production cross sections, is crucial. Such data are also required in other fields of nuclear science and technology [4]. With the aim of developing a comprehensive database on (n,n′γ) reactions, prompt gamma rays induced by fission neutrons on carbon, oxygen, aluminum, chlorine, calcium, titanium, iron, copper, indium, cerium and terbium were measured with the FaNGaS instrument and their associated fission-neutron spectrum-averaged production cross sections were determined [2, 3, 5–8]. Relative intensities of the gamma rays were found to agree reasonably with the values provided

✉ Eric Mauerhofer
e.mauerhofer@fz-juelich.de

[1] Jülich Centre for Neutron Science, Forschungszentrum Jülich GmbH, 52425 Jülich, Germany

[2] Lehrstuhl für Experimentalphysik IVc, RWTH Aachen University, 52056 Aachen, Germany

[3] Heinz Maier-Leibnitz Zentrum (MLZ), Technische Universität München, 85747 Garching, Germany

[4] Mathematisch-Naturwissenschaftliche Fakultät, Universität zu Köln, 50923 Cologne, Germany

by the only existing database for (n,n′γ) reactions: the "Atlas of Gamma-ray spectra from the Inelastic Scattering of Reactor Fast Neutrons" published by Demidov et al. in 1978 [9]. However, our measurements performed at FRM II show the need for a careful reevaluation of the data compiled in [9].

In the present work, the results from the measurement of gamma rays induced by interaction of fission neutrons with nickel and zirconium are presented and compared to the data given in [9]. Additionally, the elemental detection limits for both elements are given.

Theory

Prompt gamma rays induced by inelastic scattering and radiative capture reactions, i.e. (n,n′γ) and (n,γ) reactions, of fission neutrons on nickel and zirconium isotopes and by fast neutron capture reactions like ^{58}Ni(n,pγ)^{58}Co and ^{58}Ni(n,npγ)^{57}Co were measured. The integral rate $\langle \boldsymbol{R} \rangle$ (atom^{-1} s^{-1}) and the effective (spectrum-averaged) cross sections σ (cm^2) of the aforementioned reactions were estimated as follows:

$$\langle R \rangle = \sum_i \sigma(E_i) \cdot \Phi(E_i) \tag{1}$$

and:

$$\langle \sigma \rangle = \frac{\langle R \rangle}{\sum_i \Phi(E_i)} \tag{2}$$

where $\Phi(E_i)$ is the neutron flux in the neutron energy bin i and $\sigma(E_i)$ the reaction cross section averaged over the neutron energy bin i. The neutron-energy spectrum determined at sample position by means of the foil activation technique [2] is shown in Figs. 1 and 2. The neutron flux for each energy bin is given in Table 1 in the supplementary materials. The fission neutrons generated by the converter passed through a series of materials (1.7 mm H_2O, 2.5 mm D_2O, 2 cm Al–Mg alloy, 3 m air, 5 cm Pb and 1 cm B_4C) that down scattered a small fraction of the neutrons making the low-energy side of the spectrum harder compared to a pure ^{235}U fission spectrum [10]. The average neutron energy is calculated to 2.18 ± 0.06 MeV which is significantly higher than the expected value of 2.00 ± 0.01 MeV [11]. This may be due to the coarse energy binning used in the determination of the neutron energy spectrum. The spectrum is split into three regions defined as thermal (10^{-10} MeV $< E_i <$ 1.42 10^{-7} MeV), epithermal (1.42 10^{-7} MeV $< E_i <$ 0.06 MeV) and fast (0.06 MeV $< E_i <$ 20 MeV) with the respective fluxes, $(9.4 \pm 2.8) \times 10^2$ cm^{-2} s^{-1}, $(1.85 \pm 0.09) \times 10^6$ cm^{-2} s^{-1} and $(1.40 \pm 0.05) \times 10^8$ cm^{-2} s^{-1}. The integral neutron flux is $(1.42 \pm 0.05) \times 10^8$ cm^{-2} s^{-1}. The limits of the regions were chosen to match the binning of the calculations. The $\sigma(E_i)$-values of the investigated reactions were generated from the ENDF/B-VIII.0 [12] nuclear data library using the RECONR, BROADR and GROUPR modules of the NJOY Nuclear Data Processing System (Version 2016) [13, 14]. Their neutron-energy dependence is shown together with the neutron-energy spectrum in Fig. 1. The integral reaction rates R and the effective cross sections σ obtained by means of Eqs. (1) and (2), respectively, for the epithermal and fast region of the neutron spectrum are given in Table 1. The rates of (n,γ) reactions induced by thermal neutrons were neglected because of the low thermal neutron flux. The effective cross sections obtained for the fast neutrons σ_{fast} are

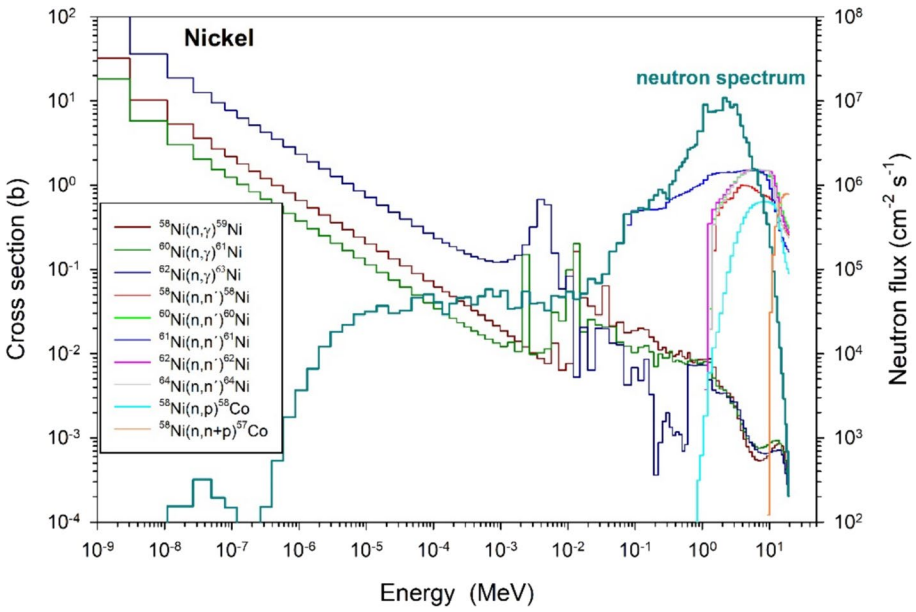

Fig. 1 Neutron-energy spectrum at sample position (right scale of y-axis) and neutron-energy dependence of the grouped microscopic cross section $\sigma(E_i)$ averaged over the neutron-energy bin i for the investigated reactions on nickel

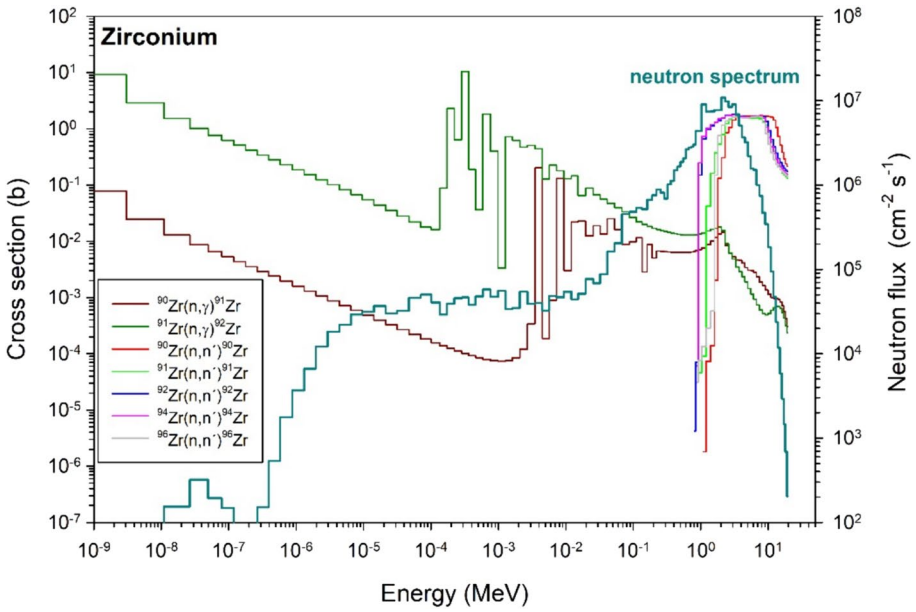

Fig. 2 Neutron-energy spectrum at sample position (right scale of *y*-axis) and neutron-energy dependence of the grouped microscopic cross section $\sigma(E_i)$ averaged over the neutron-energy bin *i* for the investigated reactions on zirconium

Table 1 Reactions rates *R* and effective cross sections ‹σ› for the investigated reactions calculated by mean of Eqs. (1) and (2), respectively

Neutron-energy range	1.4 10^{-7}–0.06 MeV (epithermal)		0.06–20 MeV (fast)		10^{-10}–20 MeV (integral)	
Φ	1.85(9) 10^{6} cm^{-2} s^{-1}		1.40(5) 10^{8} cm^{-2} s^{-1}		1.42(5) 10^{8} cm^{-2} s^{-1}	
	$<\sigma_{epi}>$ (mb)	R (atom^{-1} s^{-1})	$<\sigma_{fast}>$ (mb)	R (atom^{-1} s^{-1})	$<\sigma_{int}>$ (mb)	R (atom^{-1} s^{-1})
Nickel						
^{58}Ni(n,γ)^{59}Ni	59(8)	1.1(2) 10^{-19}	5.4(7) 6.25[a]	8(1) 10^{-19}	6.2(8)	9(1) 10^{-19}
^{60}Ni(n,γ)^{61}Ni	45(7)	8(2) 10^{-20}	4.8(6) 5.43[a]	6.7(9) 10^{-19}	5.4(7)	8(1) 10^{-19}
^{61}Ni(n,γ)^{62}Ni	155(28)	2.9(6) 10^{-19}	3.7(5) 5.02[a]	5.1(7) 10^{-19}	5.7(7)	8(1) 10^{-19}
^{62}Ni(n,γ)^{63}Ni	211(30)	3.9(7) 10^{-19}	3.6(4) 3.80[a]	5.1(7) 10^{-19}	6.4(7)	9(1) 10^{-19}
^{64}Ni(n,γ)^{65}Ni	32(5)	6(1) 10^{-20}	2.0(2) 2.24[a]	2.8(4) 10^{-19}	2.4(3)	3.4(5) 10^{-19}
^{58}Ni(n,n′)^{58}Ni			435(36) 379[a]	6.1(7) 10^{-17}	429(35)	6.1(7) 10^{-17}
^{60}Ni(n,n′)^{60}Ni			601(49) 528[a]	8.4(9) 10^{-17}	593(49)	8.4(9) 10^{-17}
^{61}Ni(n,n′)^{61}Ni			1250(121) 1205[b]	1.8(2) 10^{-16}	1234(120)	1.8(2) 10^{-16}
^{62}Ni(n,n′)^{62}Ni			638(53) 568[a]	8.9(9) 10^{-17}	630(53)	8.9(9) 10^{-17}
^{64}Ni(n,n′)^{63}Ni			578(47) 547[b]	8.1(9) 10^{-17}	571(47)	8.1(9) 10^{-17}
^{58}Ni(n,p)^{58}Co	–	–	119(9) 107[a]	1.7(2) 10^{-17}	117(9)	1.7(2) 10^{-17}
^{58}Ni(n,np)^{57}Co			0.46(4) 0.32[a]	6.4(7) 10^{-20}	0.45(4)	6.4(7) 10^{-20}
Zirconium						
^{90}Zr(n,γ)^{91}Zr	15(3)	2.8(6) 10^{-20}	7.8(8) 7.8[a]	1.1(1) 10^{-18}	7.8(8)	1.1(1) 10^{-18}
^{91}Zr(n,γ)^{92}Zr	508(80)	9(2) 10^{-19}	11(1) 12[a]	1.5(2) 10^{-18}	17(2)	2.4(3) 10^{-18}
^{92}Zr(n,γ)^{93}Zr	48(9)	9(2) 10^{-20}	13(1) 14[a]	1.8(2) 10^{-18}	13(2)	1.9(3) 10^{-18}
^{94}Zr(n,γ)^{95}Zr	27(5)	5(1) 10^{-20}	9(1) 9.5[a]	1.2(2) 10^{-18}	9(1)	1.3(3) 10^{-18}
^{96}Zr(n,γ)^{97}Zr	479(72)	9(2) 10^{-19}	8(1) 7.9[a]	1.1(1) 10^{-18}	14(2)	2.0(3) 10^{-18}
^{90}Zr(n,n′)^{90}Zr	–	–	569(49) 494[a]	7.9(8) 10^{-17}	562(45)	7.9(8) 10^{-17}
^{91}Zr(n,n′)^{91}Zr	–	–	704(57) 689[b]	1.0(1) 10^{-16}	695(57)	1.0(1) 10^{-16}
^{92}Zr(n,n′)^{92}Zr	–	–	1098(95) 995[b]	1.5(1) 10^{-16}	1084(94)	1.5(1) 10^{-16}
^{94}Zr(n,n′)^{94}Zr	–	–	1112(96) 1004[b]	1.6(2) 10^{-16}	1098(96)	1.6(2) 10^{-16}
^{96}Zr(n,n′)^{96}Zr	–	–	739(60) 642[b]	1.0(1) 10^{-16}	729(59)	1.0(1) 10^{-16}

Φ is the neutron flux in the considered neutron-energy region. [a]cross sections from ENDF/B-VIII.0 library evaluated in JANIS for a fission spectrum (kT = 1.35 MeV) [15]. [b]cross sections calculated from JENDL-4.0 [16, 17]

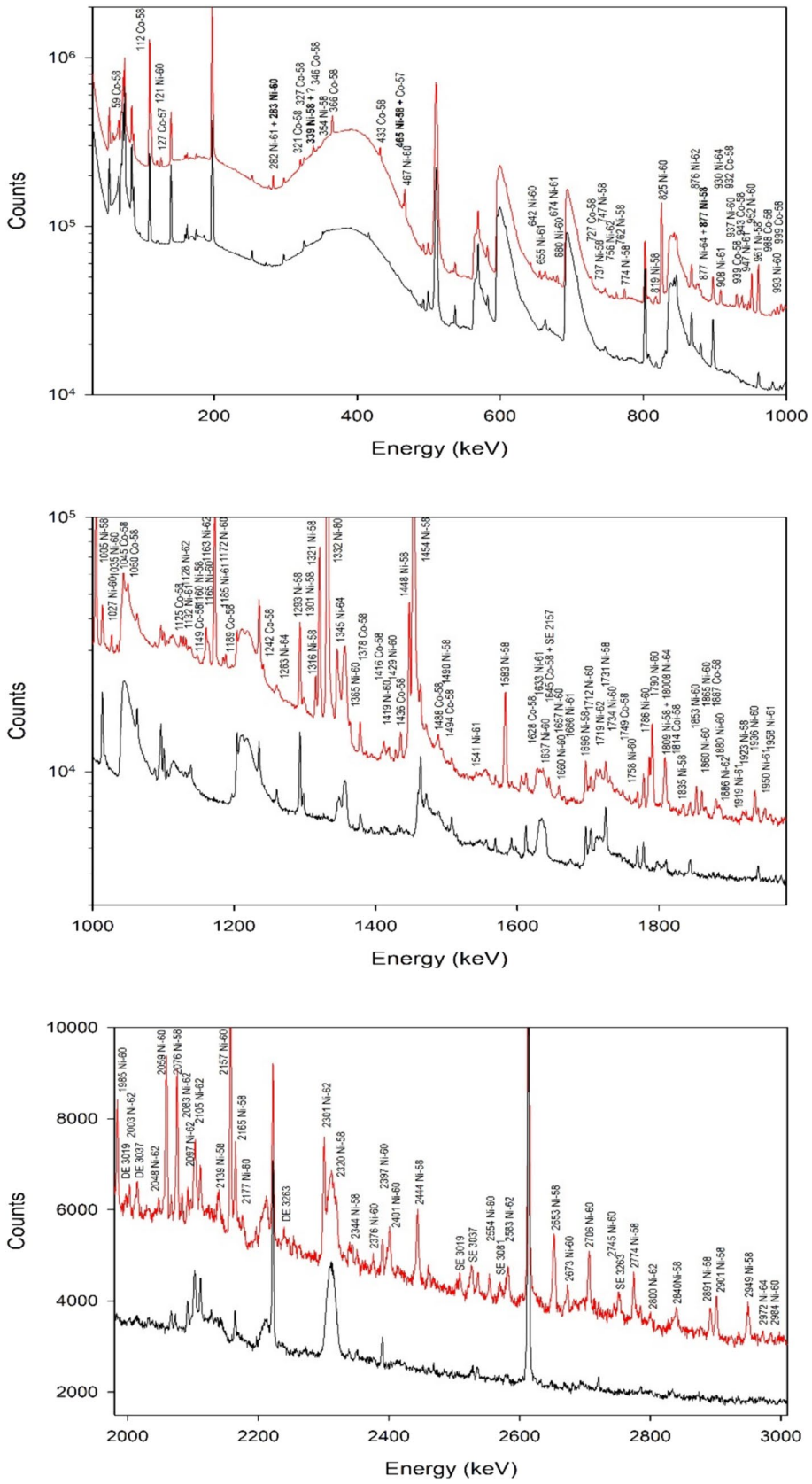

Fig. 3 Gamma-ray spectra in the energy range 30–3000 keV recorded during 25,220 s for nickel (red) and 46,454 s for the beam background (black). Prompt gamma rays issued from (n,γ) reactions are written in bold. (Color figure online)

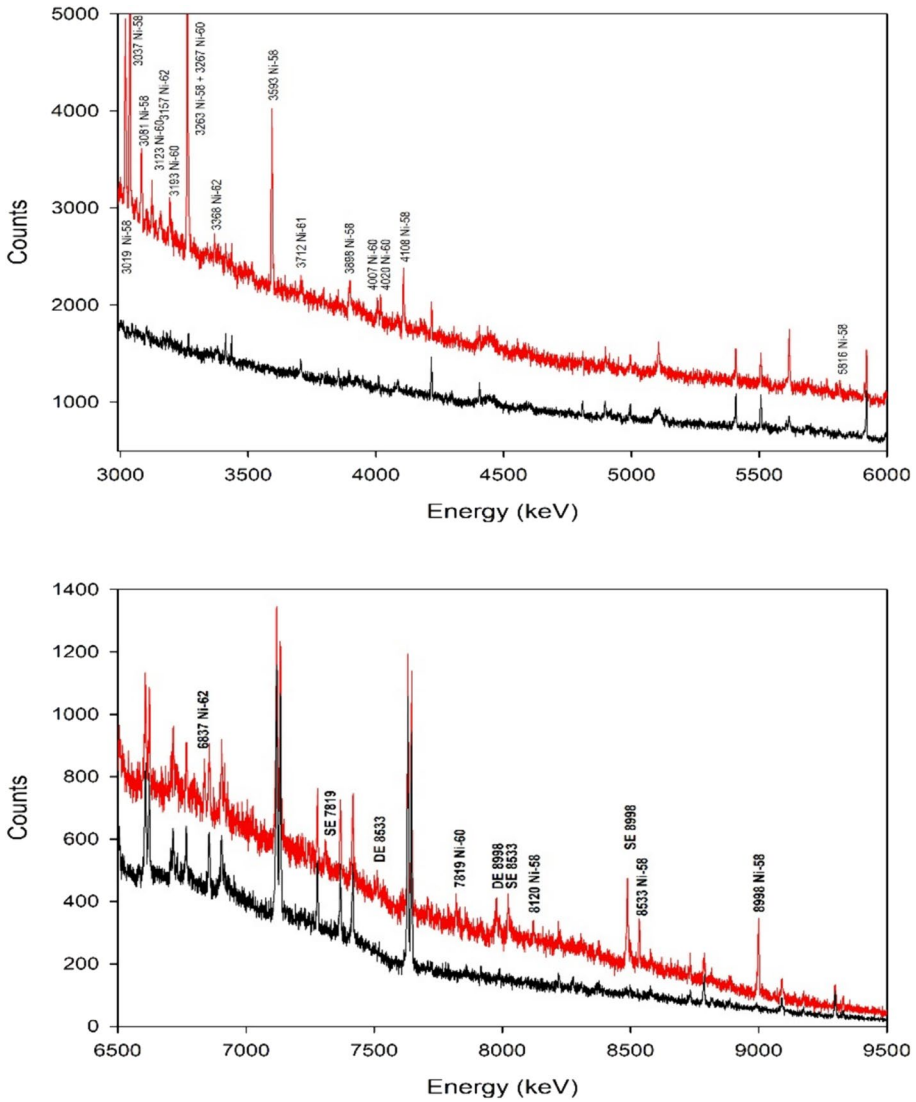

Fig. 4 Gamma-ray spectra in the energy range 3000–9500 keV recorded during 25,220 s for nickel (red) and 46,454 s for the beam background (black). Prompt gamma rays issued from (n,γ) reactions are written in bold. (Color figure online)

comparable with the values evaluated for a fission spectrum (kT = 1.35 MeV) given in JANIS (java-based nuclear data information software) Book of neutron-induced cross sections [15]. The differences might be related to the deviation of the fission neutron spectrum from a Watt spectrum. The (n,γ) reaction is mainly induced by the fast neutrons for ^{58}Ni, ^{60}Ni, ^{64}Ni, ^{90}Zr, ^{92}Zr and ^{94}Zr. In the case of ^{61}Ni, ^{62}Ni, ^{91}Zr and ^{96}Zr the rates produced by capture of epithermal and fast neutrons represent roughly 40% and 60% of the total rate, respectively. The rates of the (n,n′)-reactions for nickel and zirconium isotopes are roughly two orders of magnitude higher than the corresponding (n,γ)-reactions rates. The rates of the ^{58}Ni(n,p)^{58}Co and ^{58}Ni(n,np)^{57}Co reactions are 3.5 and 950 times lower than the rate of the ^{58}Ni(n,n′)^{58}Ni reaction.

Experimental

Prompt gamma radiation generated by fission neutrons on pure nickel ($m = 2.81$ g, $S = 3.5 \times 3.5$ cm^2) and zirconium ($m = 1.11$ g, $S = 2.6 \times 2.6$ cm^2) foils of natural composition was investigated with the FaNGaS set-up described in [2]. The foils with a thickness of 0.025 cm were irradiated with their surface perpendicular to the neutron beam of quadratic shape (6×6 cm^2). The fast-neutron flux at sample position was $(1.40 \pm 0.05) \times 10^8$ cm^{-2} s^{-1}. The irradiation time was 10 h for nickel and 14.5 h for zirconium. The gamma-ray spectra were collected during neutron irradiation for 7 h and 11.4 h (live times), respectively. The measurement was performed at an angle of 90° between neutron beam axis and spectrometer and with a sample-to-detector distance of 67 cm. The spectra were analyzed with the software HYPERMET-PC [18]. Previous beam background analysis [2] was considered for identification and correction of possible interferences. The spectra of

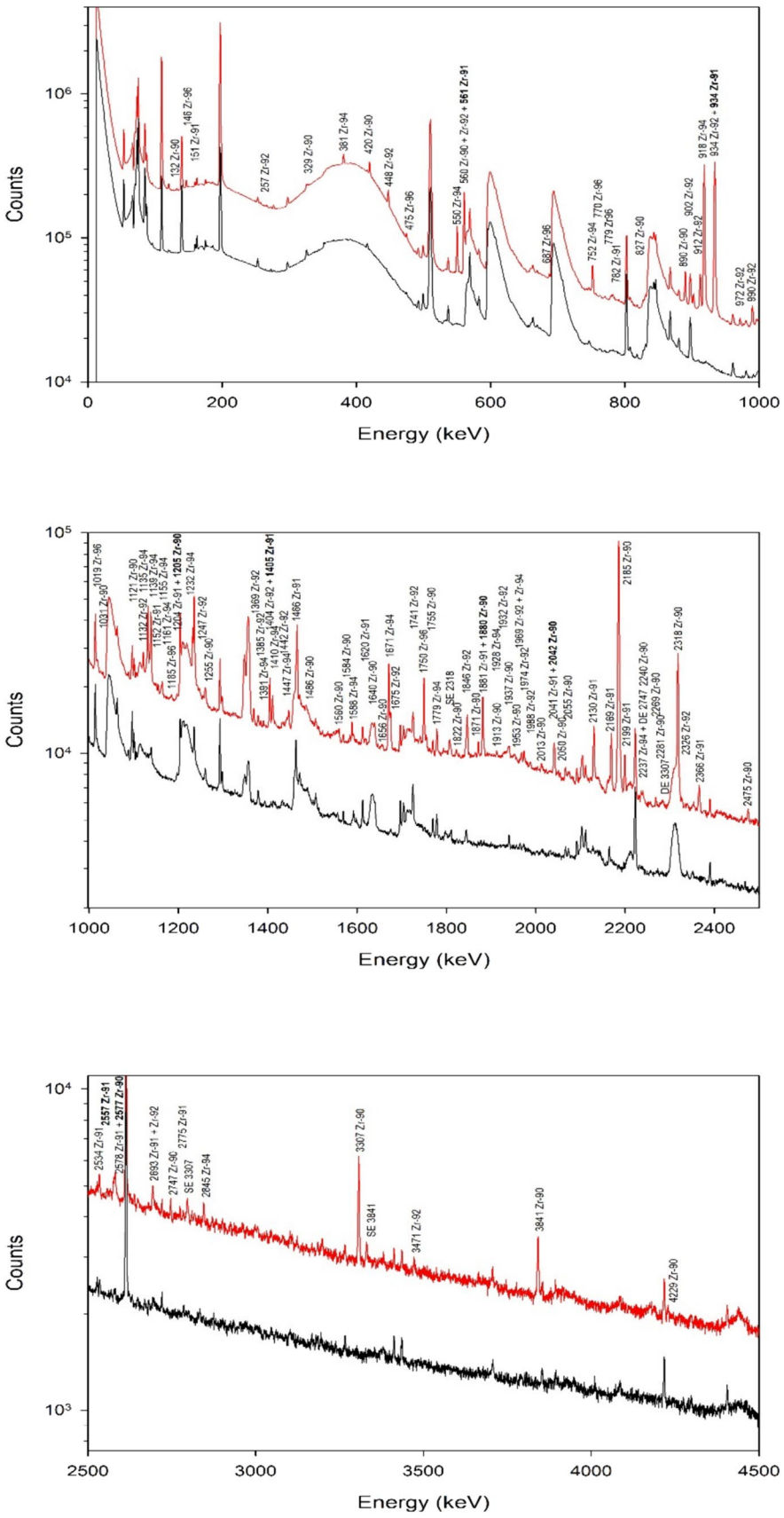

Fig. 5 Gamma-ray spectra in the energy range 0–4500 keV recorded during 41,028 s for zirconium (red) and 46,454 s for the beam background (black). Prompt gamma rays issued from (n,γ) reactions are written in bold. (Color figure online)

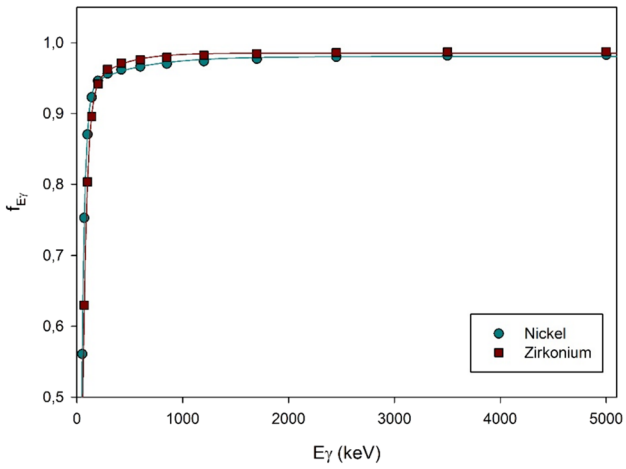

Fig. 6 Dependence of the gamma-ray self-absorption factor $f_{E\gamma}$ on the gamma energy E_γ for the nickel and zirconium foils. The solid lines represent the fit of the data with Eq. (4). (Color figure online)

the nickel and zirconium foils are shown together with the beam background in Figs. 3, 4 and 5, respectively. Due to the scattering of fission neutrons towards the detector, the count rates of background lines are increased by a mean factor of 1.39 ± 0.19 for nickel and 1.21 ± 0.02 for zirconium. These factors were used to correct possible background interferences. Identification of the gamma rays issued from inelastic scattering as well from capture of fission neutrons was done using the database NutDat 3.0 [19] and nuclear data provided in [20–30]. The PGNAA database [31] was used to check the presence of gamma rays from (n,γ) reactions and possible related interferences.

Method

The net peak area $P_{E\gamma}$ of a prompt gamma ray measured at the energy E_γ can be given by:

$$P_{E\gamma} = \frac{m}{M} N_A h \varepsilon_{E\gamma} \langle \sigma_{E\gamma} \rangle \Phi t_c f_n f_{E\gamma} \tag{3}$$

where m (g) is the amount of element, M (g mol^{-1}) the molar mass of the element, N_A the Avogadro number, h the abundance of the isotope considered, $\varepsilon_{E\gamma}$ the full-energy-peak efficiency, $\sigma_{E\gamma}$ (cm^2) the effective isotopic cross section for gamma-ray production, Φ (cm^{-2} s^{-1}) the neutron flux, t_c the counting live time (s) f_n the neutron self-shielding factor and $f_{E\gamma}$ the gamma-ray self-absorption factor. As the foils were very thin, the corrections for neutron absorption and multiple scattering were neglected, i.e. $f_n \approx 1$. The gamma-ray self-absorption of the foils was determined numerically using the Monte Carlo transport simulation code PHITS (Particle and Heavy Ion Transport code System) Version 3.02 [32] as described in [6]. The dependence of the factor for gamma-ray self-absorption $f_{E\gamma}$ on the gamma energy E_γ is shown in Fig. 6 and was approximated to the following semi-empirical function:

$$f_{E\gamma} = a_0 + a_1 \cdot \left(1 - e^{-a_2 \cdot E_\gamma}\right) + a_3 \cdot \left(1 - e^{-a_4 \cdot E_\gamma}\right) \tag{4}$$

with $a_0 = -1.1448$, $a_1 = 2.0756$, $a_2 = 0.0343$, $a_3 = 0.0497$ and $a_4 = 2.0917 \cdot 10^{-3}$ for the nickel foil, $a_0 = -1.1170$, $a_1 = 2.0326$, $a_2 = 0.0272$, $a_3 = 0.0698$ and $a_4 = 3.5614 \cdot 10^{-3}$ for the zirconium foil and E_γ in keV.

Possible interferences from prompt gamma rays induced by (n,γ)-reactions were evaluated by means of Eq. (3) setting the isotopic abundance to one ($h = 1$) and using, instead of the isotopic cross section $\sigma_{E\gamma}$, the elemental cross section $\sigma^Z_{E\gamma}$ which is estimated as

$$\left\langle \sigma^Z_{E\gamma} \right\rangle = \sigma^Z_{E\gamma,\mathrm{th}} \cdot \frac{\langle \sigma_0 \rangle}{\sigma_{0,\mathrm{th}}} \tag{5}$$

where $\sigma^Z_{E\gamma,th}$ is the elemental cross section for production of prompt gamma rays by thermal neutron capture [31], $\sigma_{0,\mathrm{th}}$ the elemental thermal neutron capture cross section ($\sigma_{0,\mathrm{th}} = 4.39 \pm 0.15$ b for nickel, $\sigma_{0,\mathrm{th}} = 190 \pm 30$ mb for zirconium [31]) and σ_0 the effective elemental cross section derived from the isotopic cross sections $\langle \sigma_{\mathrm{int}} \rangle$ given in column 6 of Table 1. The resulting values of $\langle \sigma_0 \rangle$ are 6 ± 1 mb for nickel and 10 ± 2 mb for zirconium.

The intensity of the gamma rays of nickel and zirconium, respectively, were calculated relative to the element-specific reference gamma line used in [9]. The relationship between the measured intensities (I_R) and the intensities (I_{RD}) determined in [9] was analyzed with the following semi-empirical function:

$$I_R = a \cdot \left(I_{RD}\right)^b \tag{6}$$

with a and b the coefficients obtained by the fit of the data. Additionally, the consistency between the two sets of data was deduced from the distribution of the residuals in unit of standard deviation [σ], calculated, as:

$$r = \frac{I_R - I_{RD}}{\sqrt{\left(s_{I_R}\right)^2 + \left(s_{I_{RD}}\right)^2}} \tag{7}$$

with s is the absolute uncertainty of the intensity.

Gamma rays induced in nickel

One hundred sixty-seven prompt gamma lines from the interaction of fission neutrons with nickel were identified, 128 associated to (n,n′γ)-, 32 to ^{58}Ni(n,pγ)^{58}Co-, 5 to (n,γ)- and 2 to ^{58}Ni(n,n + pγ)^{57}Co-reactions. From the 128 (n,n′γ)

Table 2 Gamma rays of ^{58}Ni induced by inelastic scattering of fission neutrons

This work				From Demidov Atlas [9]		r
E_γ (keV)	$P_{E\gamma}/\varepsilon_{E\gamma}.f_{E\gamma}(\times 10^{-8})$ (Count)	I_R(relative) (%)	$\langle\sigma_{E\gamma}(90°)\rangle$(mb)	E_γ (keV)	I_{RD}(relative) (%)	
354.5 ± 0.1	1.00 ± 0.10	0.43 ± 0.01	1.44 ± 0.05	354.4 ± 0.8	0.45 ± 0.10	− 0.20
737.2 ± 0.2	0.40 ± 0.06	0.17 ± 0.03	0.58 ± 0.09	738.1 ± 0.8	0.25 ± 0.10	− 0.77
762.34 ± 0.07	0.64 ± 0.05	0.27 ± 0.02	0.92 ± 0.08	762.9 ± 0.8	0.30 ± 0.10	− 0.29
818.9 ± 0.1	0.93 ± 0.31	0.40 ± 0.13	1.34 ± 0.45	817.8 ± 0.6	0.6 ± 0.2	− 0.83
960.71 ± 0.03	7 ± 2	3.0 ± 0.9	10 ± 3	961.3 ± 0.2	3.7 ± 0.5	− 0.68
1004.65 ± 0.03	24.9 ± 0.8	10.6 ± 0.5	36 ± 2	1004.80 ± 0.15	12.3 ± 0.1	− 3.33
1160.33 ± 0.05	6.55 ± 0.20	2.78 ± 0.11	9.40 ± 0.44	1161.7 ± 0.3	3.3 ± 0.8	− 0.64
1301.3 ± 0.3	0.67 ± 0.07	0.29 ± 0.03	0.99 ± 0.11			
1315.82 ± 0.08	2.80 ± 0.10	1.19 ± 0.06	4.04 ± 0.20	1316.9 ± 0.4[a]	2.3 ± 0.10	− 9.51
1320.56 ± 0.03	21.5 ± 0.7	9.19 ± 0.40	31 ± 1	1321.4 ± 0.2	8.7 ± 0.12	1.20
1447.82 ± 0.08	14.1 ± 0.5	6.02 ± 0.28	20 ± 1	1448.6 ± 1.0[b]	9.9 ± 0.20	− 11.28
1453.63 ± 0.03	234 ± 7	100.00	338 ± 16	1454.28 ± 0.10	100	–
1490 ± 0.3	0.65 ± 0.06	0.28 ± 0.03	0.95 ± 0.09	1490.1 ± 0.9[c]	0.55 ± 0.15	− 0.65
1583.04 ± 0.04	6.23 ± 0.20	2.66 ± 0.12	9.00 ± 0.43	1583.7 ± 0.3	2.6 ± 0.3	0.19
1696.4 ± 0.4	0.51 ± 0.20	0.22 ± 0.09	0.74 ± 0.29	1697.5 ± 0.9	0.30 ± 0.10	− 0.59
1731.4 ± 0.2	0.40 ± 0.04	0.17 ± 0.02	0.58 ± 0.06			
1809.6 ± 0.2	2.11 ± 0.18	0.90 ± 0.08	3.06 ± 0.28	1809.5 ± 0.3[d]	1.4 ± 0.2	− 2.32
1834.6 ± 0.3	0.42 ± 0.05	0.18 ± 0.02	0.61 ± 0.07			
1923.4 ± 0.3	0.27 ± 0.05	0.11 ± 0.02	0.38 ± 0.07			
2059.38 ± 0.05	2.35 ± 0.10	1.00 ± 0.05	3.40 ± 0.19	2059.8 ± 0.8	0.8 ± 0.3	0.66
2075.80 ± 0.05	2.09 ± 0.08	0.89 ± 0.04	3.02 ± 0.16	2077.0 ± 0.5	0.9 ± 0.2	− 0.05
2138.49 ± 0.03	0.82 ± 0.07	0.35 ± 0.03	1.18 ± 0.11	2139.4 ± 0.6	0.30 ± 0.10	0.48
2164.84 ± 0.05	0.91 ± 0.05	0.39 ± 0.02	1.31 ± 0.08	2167.1 ± 0.8	0.45 ± 0.15	− 0.39
2320.2 ± 0.3	1.11 ± 0.07	0.47 ± 0.03	1.60 ± 0.11	3322.8 ± 0.10	0.30 ± 0.10	1.63
2343.8 ± 0.2	0.28 ± 0.04	0.12 ± 0.02	0.40 ± 0.06			
2443.65 ± 0.07	1.94 ± 0.10	0.83 ± 0.05	2.80 ± 0.17	2444.4 ± 0.6	1.1 ± 0.2	− 1.31
2461.0 ± 0.9	0.33 ± 0.07	0.14 ± 0.03	0.47 ± 0.10			
2652.7 ± 0.1	2.14 ± 0.10	0.91 ± 0.05	3.09 ± 0.18	2652.9 ± 0.6	1.0 ± 0.2	− 0.44
2774.52 ± 0.08	0.91 ± 0.06	0.39 ± 0.03	1.31 ± 0.10	2776.1 ± 0.13	0.50 ± 0.15	− 0.72
2839.6 ± 0.3	0.97 ± 0.08	0.41 ± 0.04	1.40 ± 0.12	2841.1 ± 0.10	0.35 ± 0.10	0.56
2891.9 ± 0.3	0.71 ± 0.04	0.30 ± 0.02	1.03 ± 0.07	2893.6 ± 0.12	0.5 ± 0.2	− 0.99
2901.1 ± 0.1	1.02 ± 0.05	0.43 ± 0.03	1.47 ± 0.09	2904.1 ± 0.12	0.45 ± 0.15	− 0.13
2949.3 ± 0.1	1.11 ± 0.07	0.47 ± 0.03	1.60 ± 0.11	2951.6 ± 0.8	0.45 ± 0.10	0.19
3019.3 ± 0.2	2.55 ± 0.20	1.09 ± 0.09	3.69 ± 0.32	3021.1 ± 0.6	1.2 ± 0.2	− 0.50
3036.77 ± 0.04	4.08 ± 0.20	1.74 ± 0.10	5.89 ± 0.36	3037.5 ± 0.8	1.6 ± 0.4	0.34
3081.4 ± 0.2	1.21 ± 0.07	0.52 ± 0.03	1.75 ± 0.12	3083.7 ± 0.15	0.60 ± 0.15	− 0.52
3262.6 ± 0.1	3.98 ± 0.20	1.70 ± 0.10	5.75 ± 0.35	3263.6 ± 0.6	1.7 ± 0.3	0
3592.64 ± 0.06	2.96 ± 0.10	1.26 ± 0.06	4.28 ± 0.21	3593.6 ± 0.10	1.3 ± 0.3	− 0.13
3897.7 ± 0.3	0.71 ± 0.06	0.30 ± 0.03	1.03 ± 0.09	3896.1 ± 0.20	0.35 ± 0.15	− 0.33
4108.1 ± 0.2	1.53 ± 0.10	0.65 ± 0.05	2.21 ± 0.16	4109.3 ± 0.15	0.8 ± 0.3	− 0.49
5816 ± 1	0.43 ± 0.08	0.18 ± 0.03	0.62 ± 0.12			

$E\gamma$ is the gamma-ray energy, $P_{E\gamma}/\varepsilon_{E\gamma}.f_{E\gamma}$ the net count in the gamma-ray peak divided by the full-energy-peak efficiency and the gamma-ray self-absorption factor,I_R the relative intensity of the gamma-ray and $\langle\sigma_{E\gamma}(90°)\rangle$ the fission-neutron spectrum-averaged isotopic cross section for gamma ray production at an angle of 90° between neutron beam and detector determined with Eq. (3). r is the residual calculated by means of Eq. (7)

[a]not well resolved from the 1321-keV line

[b]not well resolved from the 1454-keV line

[c]Probably doublet with 1488-keV (^{58}Co)

[d]Probably doublet with 1808-keV (^{64}Ni)

reactions 41 lines were assigned to ^{58}Ni, 48 to ^{60}Ni, 15 to ^{61}Ni, 18 to ^{62}Ni and 6 to ^{64}Ni. Concerning the 5 (n,γ)-lines, 3 were associated to ^{58}Ni, 2 to ^{60}Ni and 1 to ^{62}Ni. The gamma rays are listed in Tables 2, 3, 4, 5, 6, 7 and 8, respectively. All lines given in [9] were detected except the weak lines of ^{58}Co at 312.9 keV from the 365.7-keV level [21] and of ^{58}Ni at 383.5 keV from the 3420.4-keV level [21] due to the high background at the corresponding energies. These lines are reported in the NuDat 3.0 database and the fact that the strongest gamma from each level (365.6 keV for ^{58}Co, 961.3 keV for ^{58}Ni) were also detected in our measurement makes Demidov's assignments plausible. Additional lines, which are mentioned in NuDat 3.0, were identified in our spectrum:

- 1301.3, 1731.4, 1834.6, 1923.4, 2343.8, 2461.0 and 5816 keV for ^{58}Ni,
- 120.9, 936.5, 1035.3, 1165.1, 1364.9, 1418.9, 1428.9, 1637.7, 1657.4, 1660.0, 1711.7, 1743.3, 1758.4, 1865.2, 2177.1, 2376.5, 2673.1, 2397.3, 2554.2, 2745.0, 4007.2, 4019.6 keV for ^{60}Ni,
- 947.3, 1131.7, 1184.8, 1541.6, 1633.1, 1666.5, 1918.8, 1958.0, 2581.6, and 3711.9 keV for ^{61}Ni,
- 755.7, 875.6, 1128.2, 1163.2, 1717.8, 1172.4, 1885.9, 2002.7, 2047.7, 2083.3, 2096.5, 2105.3, 2300.6, 2351.2, 2582.8, 2799.7 and 3368.5 keV for ^{62}Ni,
- 878.2, 1263.3, 1807.7 and 2971.6 keV for ^{64}Ni,
- 58.7, 111.8, 727.5, 932.2, 943.2, 987.8, 999.1, 1148.7, 1242.1, 1416.2, 1435.5, 1488.2, 1493.9, 1628.5, 1645.21, 1749.4, 1814.0 and 1867.9 keV for ^{58}Co.

The counts of radiative capture lines calculated by means of Eqs. (1) and (2) are compared with the measured values in Table 8. For the lines at 6837.5, 7819.5, 8120, 8533.5 and 8999.4 keV, the calculated and the measured values agree with each other by taking into account their respective uncertainties. This result indicates the reliability of the determined effective cross section of nickel and that the branching ratios of radiative capture lines seem to be independent of the neutron energy as previously observed in our work on indium [6]. The lines at 282.9 and 877.9 keV were found to interfere significantly with the (n,n′γ)-lines of ^{61}Ni and ^{64}Ni at same energy with contributions to the net counts of 9 ± 2 and 25 ± 2%, respectively. In the case of the 339.4- and 464.9-keV lines, radiative capture contributes to 8 ± 1 and 65 ± 12% of the net counts indicating they are also produced by additional reactions, but other than (n,n′γ)- or (n,pγ)- reactions as for the latter no gamma rays at the corresponding energies are reported in NuDat 3.0. Note that an unassigned strong line at 339 keV can also be observed in the nickel spectrum measured by Demidov et al. [9]. In addition, the energy resolution of their detector was not good enough to detect a line at 465 keV close to the 466-keV line of ^{60}Ni. Concerning the 126.8-keV line detected in our spectrum, we exclude the fact that it could correspond to the delayed line at 127.1 keV ($I_{E\gamma}$ = 16.7% [19]) of ^{57}Ni ($T_{1/2}$ = 35.60 h) induced by ^{58}Ni(n,2n)^{57}Ni due to the very low value of the fission spectrum averaged cross section of this reaction, 7.0 ± 0.6 µb [15]. Therefore, according to Nudat 3.0, this line as well as the 464.9-keV line could probably be associated to ^{57}Co produced by the ^{58}Ni(n,np)^{57}Co reaction. The energy threshold of this reaction is around 8 MeV [15] and the effective activation flux integrated in the range 8 to 20 MeV is 7.1 ± 0.3 10^5 cm^{-2} s^{-1}. However, the 127-keV line is not detected in Demidov's measurement probably due to a lower neutron flux above 8 MeV in their reactor neutron spectrum.

The intensities of the gamma lines were calculated using the 1454-keV line as reference (100%), and they were compared with the values determined in [9] in Tables 2, 3, 4, 5, 6 and 7. The relationship between the intensities is shown in Fig. 7 and is expressed by Eq. (6) with $a = 0.88 \pm 0.03$ and $b = 0.97 \pm 0.03$. The histogram of the residuals r calculated from Eq. (7) is given in Fig. 7. The fit of the histogram with a Gaussian shows an agreement between the data at the 0.7σ level, indicating a good consistency. The fission-neutron spectrum-averaged isotopic cross sections for gamma-ray production calculated by means of Eq. (3) with a flux of 1.40×10^8 cm^{-2} s^{-1} are given in column 4 of Tables 2, 3, 4, 5, 6 and 7.

Gamma rays of zirconium

A total of 99 prompt gamma lines induced by inelastic scattering of fission neutrons with zirconium were identified, 31 related to ^{90}Zr, 17 to ^{91}Zr, 24 to ^{92}Zr, 19 to ^{94}Zr and 8 to ^{96}Zr (see Tables 9,10,11,12 and 13). Additionally, the delayed gamma lines at 132.7 keV (Iγ = 4.13% [24]) and 2318 9 keV (Iγ = 82.0% [24]) of the activation product ^{90m}Zr produced by the ^{90}Zr(n,n′)^{90m}Zr were observed. The capture line of ^{91}Zr at 2557 keV was detected, free of any interferences. Most of the gamma lines given in [9] were measured and additional lines that are reported in NuD at 3.0 were detected:

- 132.3, 828.0, 1255.4, 1584.1, 1755.0, 1913.0, 1937.0, 1952.6, 2013.2, 2050.3, 2054.6, 2239.9, 2280, 2269.5 keV for ^{90}Zr
- 150.8, 1068.7, 1151.6, 1619.0, 2577.5, 2774.8 keV for ^{91}Zr
- 257.2, 902.2, 1247.5, 1384.9, 1442.7, 1675.1, 1741.2, 1932.2, 1974.0, 1987.6, 2326.5, 2693.3, 2871.0, 3470.7 keV for ^{92}Zr
- 1134.9, 1154.7, 1161.1, 1390.6, 1778.6, 1928, 1968.2, 2236.5, 2845.2 keV for ^{94}Zr

Table 3 Gamma rays of ^{60}Ni induced by inelastic scattering of fission neutrons

This work				From Demidov Atlas [9]		r
E_γ (keV)	$P_{E\gamma}/\varepsilon_{E\gamma}f_{E\gamma}$ ($\times 10^{-8}$) (Count)	I_R(relative) (%)	$\langle\sigma_{E\gamma}(90°)\rangle$ (mb)	E_γ (keV)	I_{RD}(relative) (%)	
120.94 ± 0.12	0.70 ± 0.12	0.30 ± 0.05	2.63 ± 0.46			
466.52 ± 0.04	7.39 ± 0.31	3.16 ± 0.16	27.7 ± 1.5	467.1 ± 0.2	3.2 ± 0.4	− 0.09
642.18 ± 0.07	0.59 ± 0.04	0.25 ± 0.02	2.21 ± 0.16	643.1 ± 0.6	0.35 ± 0.10	− 0.98
679.86 ± 0.07	1.03 ± 0.31	0.44 ± 0.13	3.9 ± 1.1	680.7 ± 0.6	0.3 ± 0.1	0.85
746.55 ± 0.08	0.73 ± 0.07	0.31 ± 0.03	2.74 ± 0.29	746.5 ± 0.6	0.40 ± 0.10	− 0.86
825.38 ± 0.03	23.4 ± 0.7	10.0 ± 0.4	88 ± 4	826.08 ± 0.15	10.7 ± 0.8	− 0.78
936.5 ± 0.2	0.48 ± 0.05	0.20 ± 0.02	1.80 ± 0.20			
951.58 ± 0.03	5.55 ± 0.20	2.37 ± 0.11	21 ± 1	952.4 ± 0.3	2.8 ± 0.60	− 0.70
992.67 ± 0.06	1.13 ± 0.10	0.48 ± 0.04	4.24 ± 0.40	993.3 ± 0.6	0.60 ± 0.15	− 0.77
1026.92 ± 0.05	1.31 ± 0.06	0.56 ± 0.03	4.92 ± 0.28	1026.9 ± 0.8	0.4 ± 0.1	1.53
1035.3 ± 0.2	0.59 ± 0.08	0.25 ± 0.03	2.21 ± 0.31			
1165.1 ± 0.1	1.40 ± 0.09	0.60 ± 0.04	5.25 ± 0.39			
1172.42 ± 0.04[a]	28 ± 1.0	12.0 ± 0.6	37.5 ± 1.8[b]	1173.10 ± 0.15	13.3 ± 0.1	− 2.14
1292.87 ± 0.03	4.6 ± 1.1	1.96 ± 0.47	17 ± 4	1293.5 ± 0.2	2.0 ± 0.6	− 0.05
1331.92 ± 0.03	141 ± 4	60.2 ± 2.5	529 ± 24	1332.50	60 ± 5	0.04
1364.9 ± 0.2	1.17 ± 0.07	0.50 ± 0.03	4.39 ± 0.30			
1418.9 ± 0.3	0.52 ± 0.06	0.22 ± 0.03	1.95 ± 0.23			
1428.9 ± 0.4	0.51 ± 0.06	0.22 ± 0.03	1.91 ± 0.23			
1637.7 ± 0.2	0.19 ± 0.03	0.08 ± 0.01	0.73 ± 0.12			
1657.4 ± 0.8	0.17 ± 0.05	0.07 ± 0.02	0.65 ± 0.19			
1660.0 ± 0.5	0.52 ± 0.07	0.22 ± 0.03	1.91 ± 0.27			
1711.7 ± 0.2	0.35 ± 0.05	0.15 ± 0.02	1.30 ± 0.19			
1734.3 ± 0.3	0.29 ± 0.07	0.12 ± 0.04	1.12 ± 0.27			
1758.4 ± 0.3	0.15 ± 0.03	0.06 ± 0.01	0.56 ± 0.11			
1786.26 ± 0.05	2.20 ± 0.10	0.94 ± 0.05	8.25 ± 0.47	1787.8 ± 0.8	1.4 ± 0.3	− 1.51
1790.41 ± 0.04	4.29 ± 0.10	1.83 ± 0.07	16.1 ± 0.7	1791.7 ± 0.8	1.4 ± 0.3	1.39
1852.76 ± 0.06	1.05. ± 0.06	0.45 ± 0.03	3.94 ± 0.26	1853.9 ± 0.8	0.45 ± 0.15	0
1860.43 ± 0.06	0.91 ± 0.05	0.39 ± 0.03	3.41 ± 0.22	1862.4 ± 0.8	0.50 ± 0.15	− 0.72
1865.2 ± 0.4	0.32 ± 0.04	0.14 ± 0.02	1.23 ± 0.16			
1880.3 ± 0.1	0.95 ± 0.08	0.40 ± 0.04	3.56 ± 0.32	1882.5 ± 0.8	0.65 ± 0.20	− 1.22
1935.56 ± 0.08	1.07 ± 0.08	0.46 ± 0.04	4.01 ± 0.33	1936.8 ± 0.7	0.6 ± 0.2	− 0.69
1984.50 ± 0.06	1.15 ± 0.05	0.49 ± 0.03	4.31 ± 0.24	1984.6 ± 0.9	0.60 ± 0.15	− 0.72
2059.38 ± 0.05	2.35 ± 0.10	1.00 ± 0.05	8.81 ± 0.49	2059.8 ± 0.8	0.8 ± 0.3	0.66
2157.66 ± 0.04	3.46 ± 0.10	1.48 ± 0.06	13.0 ± 0.6	2158.9 ± 0.3	2.0 ± 0.4	− 1.28
2177.1 ± 0.4	0.19 ± 0.04	0.08 ± 0.02	0.73 ± 0.15			
2376.5 ± 0.8	0.29 ± 0.06	0.12 ± 0.02	1.09 ± 0.23			
2673.1 ± 0.6	0.58 ± 0.07	0.25 ± 0.03	2.27 ± 0.28			
2397.3 ± 0.7	0.43 ± 0.06	0.18 ± 0.02	1.61 ± 0.23			
2401.5 ± 0.2	0.92 ± 0.06	0.39 ± 0.03	3.45 ± 0.26	2399.5 ± 1.6[c]	1.2 ± 0.3	− 2.08
2554.2 ± 0.3	0.42 ± 0..05	0.18 ± 0.02	1.58 ± 0.07			
2706.2 ± 0.1	1.16 ± 0.07	0.49 ± 0.03	4.35 ± 0.30	2707.3 ± 1.0	0.65 ± 0.20	− 0.79
2745.0 ± 0.9	0.18 ± 0.04	0.08 ± 0.02	0.67 ± 0.15			
2984.2 ± 0.3	0.18 ± 0.03	0.08 ± 0.02	0.67 ± 0.11	2984.7 ± 0.18[d]	0.30 ± 0.10	− 2.16
3123.1 ± 0.1	0.42 ± 0.04	0.18 ± 0.02	1.58 ± 0.07	3125.6 ± 1.2	0.15 ± 0.5	0.06
3192.9 ± 0.3	0.52 ± 0.06	0.22 ± 0.03	1.95 ± 0.23	3195.4 ± 1.5	0.55 ± 0.20	− 1.63
3267.4 ± 0.2	0.99 ± 0.08	0.42 ± 0.04	3.71 ± 0.33	3270.4 ± 0.8	0.6 ± 0.2	− 0.88
4007.2 ± 0.5	0.53 ± 0.08	0.23 ± 0.03	1.98 ± 0.31			
4019.6 ± 0.7	0.49 ± 0.07	0.21 ± 0.03	1.81 ± 0.27			

Table 3 (continued)

E_γ is the gamma-ray energy, $P_{E\gamma}/\varepsilon_{E\gamma}{\cdot}f_{E\gamma}$ the net count in the gamma-ray peak divided by the full-energy-peak efficiency and the gamma-ray self-absorption factor,I_R the relative intensity of the gamma-ray and $\langle\sigma_{E\gamma}(90°)\rangle$ the fission-neutron spectrum-averaged isotopic cross section for gamma ray production at an angle of 90° between neutron beam and detector determined with Eq. (3). *r* is the residual calculated by means of Eq. (7)

[a]Contain a contribution of 1172.9 keV (^{62}Ni)

[b]Calculated with $P_{E\gamma}/\varepsilon_{E\gamma}{\cdot}f_{E\gamma} = (10 \pm 0.3)\ 10^8$ obtained using a line intensity of 7.1% relative to the 1332-keV line [22]

[c]Doublet of 2397 and 2401 keV

Table 4 Gamma rays of ^{61}Ni induced by inelastic scattering of fission neutrons

This work				From Demidov Atlas [9]		*r*
E_γ (keV)	$P_{E\gamma}/\varepsilon_{E\gamma}{\cdot}f_{E\gamma}$ ($\times 10^{-8}$) (Count)	I_R(relative) (%)	$\langle\sigma_{E\gamma}(90°)\rangle$ (mb)	E_γ (keV)	I_{RD}(relative) (%)	
282.48 ± 0.03	2.95 ± 0.58[a]	1.26 ± 0.25	210 ± 42	283.0 ± 0.2	1.8 ± 0.3	− 1.38
655.37 ± 0.04	1.06 ± 0.06	0.45 ± 0.03	91 ± 6	655.9 ± 0.5	0.4 ± 0.1	0.48
674.06 ± 0.09	0.68 ± 0.08	0.30 ± 0.03	59 ± 7	674.1 ± 0.7	0.3 ± 0.1	0
908.10 ± 0.04[b]	1.67 ± 0.58[b]	0.71 ± 0.25	178 ± 62	908.6 ± 0.6	0.6 ± 0.1	0.41
947.34 ± 0.06	0.99 ± 0.06	0.42 ± 0.03	85 ± 6			
1131.73 ± 0.06	1.26 ± 0.08	0.54 ± 0.04	109 ± 8			
1184.79 ± 0.06[c]	0.79 ± 0.04	0.34 ± 0.02	68 ± 4			
1541.6 ± 0.2	0.31 ± 0.05	0.13 ± 0.02	27 ± 4			
1633.1 ± 0.4	0.11 ± 0.03	0.05 ± 0.01	10 ± 3			
1666.5 ± 0.7	0.29 ± 0.06	0.12 ± 0.02	24 ± 5			
1918.8 ± 0.2	0.30 ± 0.04	0.13 ± 0.02	26 ± 4			
1949.5 ± 0.1	0.60 ± 0.04	0.26 ± 0.02	52 ± 4	1952.6 ± 0.1	0.30 ± 0.10	− 0.39
1958.0 ± 0.7	0.32 ± 0.05	0.14 ± 0.02	28 ± 4			
2581.6 ± 0.2	1.00 ± 0.07	0.43 ± 0.03	86 ± 7			
3711.9 ± 0.4	0.23 ± 0.04	0.10 ± 0.02	20 ± 3			

E_γ is the gamma-ray energy, $P_{E\gamma}/\varepsilon_{E\gamma}{\cdot}f_{E\gamma}$ the net count in the gamma-ray peak divided by the full-energy-peak efficiency and the gamma-ray self-absorption factor,I_R the relative intensity of the gamma-ray and $\langle\sigma_{E\gamma}(90°)\rangle$ the fission-neutron spectrum-averaged isotopic cross section for gamma ray production at an angle of 90° between neutron beam and detector determined with Eq. (3). *r* is the residual calculated by means of Eq. (7)

[a]Corrected for the contribution of the 283-keV neutron capture line

[b]Corrected for the contribution of the 909-keV line of ^{60}Ni, $P_{E\gamma}/\varepsilon_{E\gamma}{\cdot}f_{E\gamma} = (0.39 \pm 0.01)\ 10^8$ calculated using an intensity ratio of 0.017 between 909- and 826-keV lines of ^{60}Ni [22]

[c]May contain a contribution of 1184 and 1186 keV (^{62}Ni)

- 474.8, 687.4, 770,4, 779.2, 1184.9 keV for ^{96}Zr

Gamma lines given at energies 213.8, 338.0 and 1065.7 in [9] were not detected in our spectrum. It should be mentioned here that the 213.8- and 1065.7-keV lines were assigned to hafnium in [9] (^{178}Hf, ^{179}Hf, ^{180}Hf for 213.8 keV and ^{180}Hf for 1065.7 keV) due to possible impurities in the zirconium sample. Also, note that an unassigned line at around 325 keV can be observed in Demidov's spectrum that could correspond to the 325.6 keV line of ^{178}Hf. The 338-keV line was assigned to the 3076-keV 4^+ level in ^{90}Zr by Demidov, which is plausible since the 890-, and 331 keV lines deexciting the same level were identified. However, the intensity of the 388-keV line relative to the 890-keV line, 29%, is considerably higher than the reported value in NuDat 3.0, 0.9%. Thus, this line could correspond rather to the 339-keV line of ^{179}Hf. In our measurement, the neutron capture lines at 1205.6, 1880.4, 2042.2 and 2577.3 keV of ^{90}Zr and at 560.9, 934.5 and 1405.1 of ^{91}Zr were found to interfere significantly with the (n,n′γ)-lines of same energies. Their contributions to the net counts were calculated by means of Eqs. (3) and (5) (see Table 8) and were corrected accordingly. The intensities of the lines calculated relative to the 934.5-keV line of ^{92}Zr (100%) are given with the values determined in [9] in Tables 9, 10, 11, 12 and 13. The relationship between the values is expressed by the relation

Table 5 Gamma rays of ^{62}Ni induced by inelastic scattering of fission neutrons

This work				From Demidov Atlas [9]		r
E_γ (keV)	$P_{E\gamma}/\varepsilon_{E\gamma}f_{E\gamma}$ ($\times 10^{-8}$) (Count)	I_R(relative) (%)	$\langle\sigma_{E\gamma}(90°)\rangle$ (mb)	E_γ (keV)	I_{RD} (relative) (%)	
755.7 ± 0.1	0.29 ± 0.01	0.12 ± 0.02	7.85 ± 0.39			
875.55 ± 0.05	1.08 ± 0.07	0.46 ± 0.03	29 ± 2			
1128.25 ± 0.06	1.21 ± 0.08	0.52 ± 0.04	33 ± 2			
1163.2 ± 0.1	1.61 ± 0.06	0.69 ± 0.03	43 ± 2			
1717.8 ± 0.3	0.27 ± 0.04	0.11 ± 0.02	7 ± 1			
1172.42 ± 0.04	18 ± 1[a]	7.69 ± 0.48	487 ± 32			
1885.9 ± 0.2	0.67 ± 0.06	0.29 ± 0.03	18 ± 2			
2002.7 ± 0.2	0.24 ± 0.03	0.10 ± 0.02	6.5 ± 0.8			
2047.7 ± 0.8	0.20 ± 0.04	0.08 ± 0.02	5.2 ± 1.0			
2083.3 ± 0.1	0.35 ± 0.04	0.15 ± 0.02	9.5 ± 1.1			
2096.5 ± 0.1	0.37 ± 0.04	0.16 ± 0.02	10 ± 1			
2105.3 ± 0.5	0.69 ± 0.08	0.29 ± 0.03	19 ± 2			
2300.58 ± 0.05	2.27 ± 0.08	0.97 ± 0.04	61 ± 3			
2351.2 ± 0.3	0.17 ± 0.03	0.07 ± 0.02	4.60 ± 0.82			
2582.8 ± 0.4	0.80 ± 0.08	0.34 ± 0.03	22 ± 2			
2799.7 ± 0.3	0.22 ± 0.03	0.10 ± 0.02	5.96 ± 0.85			
3157.0 ± 0.6[c]	0.37 ± 0.05	0.17 ± 0.02	0.53 ± 0.07	3155.9 ± 0.12	0.20 ± 0.10	−0.39
3368.5 ± 0.3	0.26 ± 0.04	0.11 ± 0.02	7 ± 1			

E_γ is the gamma-ray energy, $P_{E\gamma}/\varepsilon_{E\gamma}f_{E\gamma}$ the net count in the gamma-ray peak divided by the full-energy-peak efficiency and the gamma-ray self-absorption factor,I_R the relative intensity of the gamma-ray and $\langle\sigma_{E\gamma}(90°)\rangle$ the fission-neutron spectru-averaged isotopic cross section for gamma ray production at an angle of 90° between neutron beam and detector determined with Eq. (3). r is the residual calculated by means of Eq. (7)

[a]corrected for the contribution of 1172.9 keV (^{60}Ni). See note b of Table 3

Table 6 Gamma rays of ^{64}Ni induced by inelastic scattering of fission neutrons

This work				From Demidov Atlas [9]		r
E_γ (keV)	$P_{E\gamma}/\varepsilon_{E\gamma}f_{E\gamma}$ ($\times 10^{-8}$) (Count)	I_R(relative) (%)	$\langle\sigma_{E\gamma}(90°)\rangle$ (mb)	E_γ (keV)	I_{RD}(relative) (%)	
878.18 ± 0.09	1.01 ± 0.10[a]	0.46 ± 0.05	107 ± 11			
930.43 ± 0.08	1.94 ± 0.09	0.83 ± 0.04	206 ± 12	931.0 ± 0.5	1.0 ± 0.2	−0.83
1263.3 ± 0.2	0.45 ± 0.04	0.19 ± 0.02	48 ± 4			
1345.37 ± 0.03	4.5 ± 0.8	1.92 ± 0.35	478 ± 87	1345.7 ± 0.3	1.8 ± 0.4	0.22
1807.7 ± 0.3	0.75 ± 0.09	0.32 ± 0.04	81 ± 10			
2971.6 ± 0.7	0.14 ± 0.05	0.06 ± 0.02	15 ± 5			

E_γ is the gamma-ray energy, $P_{E\gamma}/\varepsilon_{E\gamma}f_{E\gamma}$ the net count in the gamma-ray peak divided by the full-energy-peak efficiency and the gamma-ray self-absorption factor,I_R the relative intensity of the gamma-ray and $\langle\sigma_{E\gamma}(90°)\rangle$ the fission-neutron spectrum-averaged isotopic cross section for gamma ray production at an angle of 90° between neutron beam and detector determined with Eq. (3). r is the residual calculated by means of Eq. (7)

[a]Corrected from the contribution of the 878-keV capture line

described by Eq. (6) with $a = 1.01 \pm 0.06$ and $b = 0.95 \pm 0.03$ as shown in Fig. 8. The fit of the histogram of the residuals r with a Gaussian shows an agreement between the data at the 1.3σ level, indicating a good consistency (Fig. 8). The fission-neutron spectrum-averaged isotopic cross sections for gamma-ray production calculated by means of Eq. (3) with a flux of 1.40×10^8 cm^{-2} s^{-1} are given in column 4 of Tables 9, 10, 11, 12 and 13. From the delayed gamma rays of ^{90m}Zr at 132.7 and 2318.9 we derive a fission-neutron

Table 7 Gamma rays of ^{58}Co induced by the ^{58}Ni(n,p)^{58}Co reaction

This work				From Demidov Atlas [9]		r
E_γ (keV)	$P_{E\gamma}/\varepsilon_{E\gamma}{\cdot}f_{E\gamma}$ ($\times 10^{-8}$) (Count)	I_R(relative) (%)	$\langle\sigma_{E\gamma}(90°)\rangle$ (mb)	E_γ (keV)	I_{RD}(relative) (%)	
58.72 ± 0.02	3.26 ± 0.14	1.39 ± 0.07	4.71 ± 0.26			
111.80 ± 0.04	1.37 ± 0.05	0.58 ± 0.03	1.98 ± 0.10			
321.22 ± 0.06	2.43 ± 0.14	1.04 ± 0.07	3.51 ± 0.24	321.5 ± 0.2	1.3 ± 0.4	− 0.64
326.51 ± 0.08	0.83 ± 0.13	0.35 ± 0.06	1.20 ± 0.19	327.0 ± 0.3	0.6 ± 0.2	− 1.20
346.04 ± 0.04	0.80 ± 0.06	0.34 ± 0.03	1.16 ± 0.10	346.8 ± 0.6	0.3 ± 0.1	0.38
365.96 ± 0.02	12.70 ± 0.47	5.42 ± 0.26	18.4 ± 0.9	366.6 ± 0.2	7.0 ± 0.5	− 2.81
432.82 ± 0.04	5.89 ± 0.24	2.52 ± 0.13	8.51 ± 0.46	432.9 ± 0.2	3.7 ± 0.6	− 1.92
727.5 ± 0.2	0.65 ± 0.08	0.28 ± 0.03	0.95 ± 0.12			
773.57 ± 0.05	1.28 ± 0.06	0.55 ± 0.03	1.86 ± 0.11	774.5 ± 0.4	0.60 ± 0.15	− 0.33
932.2 ± 0.2	0.61 ± 0.07	0.26 ± 0.03	0.88 ± 0.10			
938.7 ± 0.1	1.60 ± 0.10	0.64 ± 0.04	2.31 ± 0.17	938.3 ± 0.7	0.7 ± 0.1	− 0.56
943.2 ± 0.3	0.75 ± 0.09	0.32 ± 0.04	1.08 ± 0.13			
987.8 ± 0.2	0.59 ± 0.10	0.25 ± 0.04	0.85 ± 0.15			
999.1 ± 0.3	0.62 ± 0.11	0.26 ± 0.05	0.90 ± 0.16			
1044.5 ± 0.1	2.51 ± 0.18	1.07 ± 0.08	3.63 ± 0.29	1044.7 ± 0.4	0.9 ± 0.2	0.79
1050.47 ± 0.06	1.86 ± 0.09	0.79 ± 0.04	2.69 ± 0.16	1051.0 ± 0.6	0.8 ± 0.2	− 0.05
1125.0 ± 0.2	1.33 ± 0.09	0.57 ± 0.04	1.92 ± 0.14	1125.4 ± 0.8	0.35 ± 0.15	1.42
1148.7 ± 0.2	0.47 ± 0.06	0.20 ± 0.03	0.68 ± 0.09			
1188.8 ± 0.2	1.10 ± 0.08	0.47 ± 0.04	1.59 ± 0.13	1187.1 ± 0.8	0.7 ± 0.3	− 0.76
1242.1 ± 0.2	0.50 ± 0.07	0.21 ± 0.03	0.71 ± 0.10			
1378.44 ± 0.08	1.00 ± 0.11	0.43 ± 0.05	1.44 ± 0.17	1378.1 ± 0.6	0.60 ± 0.15	− 1.07
1416.2 ± 0.2	0.28 ± 0.05	0.12 ± 0.02	0.40 ± 0.07			
1435.5 ± 0.2	1.52 ± 0.09	0.65 ± 0.04	2.20 ± 0.15			
1488.2 ± 0.4	0.70 ± 0.06	0.30 ± 0.03	1.02 ± 0.09			
1493.9 ± 0.3	0.76 ± 0.06	0.32 ± 0.03	1.09 ± 0.09			
1628.5 ± 0.2	0.24 ± 0.04	0.10 ± 0.02	0.34 ± 0.06			
1645.2 ± 0.1	0.21 ± 0.02	0.09 ± 0.01	0.30 ± 0.03			
1749.4 ± 0.7	0.25 ± 0.05	0.11 ± 0.02	0.36 ± 0.07			
1814.0 ± 0.6	0.31 ± 0.06	0.13 ± 0.02	0.45 ± 0.09			
1867.9 ± 0.8	0.27 ± 0.05	0.11 ± 0.02	0.39 ± 0.07			
126.8 ± 0.03[a]	2.04 ± 0.09	0.87 ± 0.05	2.94 ± 0.18			
464.9 ± 0.2[ab]	0.64 ± 0.22	0.27 ± 0.09	0.91 ± 0.31			

E_γ is the gamma-ray energy, $P_{E\gamma}/\varepsilon_{E\gamma}{\cdot}f_{E\gamma}$ the net count in the gamma-ray peak divided by the full-energy-peak efficiency and the gamma-ray self-absorption factor, I_R the relative intensity of the gamma-ray and $\langle\sigma_{E\gamma}(90°)\rangle$ the fission-neutron spectrum-averaged isotopic cross section for gamma ray production at an angle of 90° between neutron beam and detector determined with Eq. (3). r is the residual calculated by means of Eq. (7)

[a]cautiously assigned to ^{57}Co from ^{58}Ni(n,n + p)^{57}Co reaction

[b]Corrected from the contribution of the 465-keV capture line

spectrum-averaged cross section of 88 ± 8 mb for the ^{90}Zr(n,n′)Zr^{90m} reaction.

Detection limit

The detection limit (DL) corresponds here to the smallest amount of pure element that can be detected. It was calculated neglecting gamma self-absorption and neutron self-shielding by means of Eq. (3) using the minimum peak area $P_{E\gamma}(c)$ which is defined for the case of an interference-free gamma line by [33]:

$$P_{E\gamma}(c) = \frac{\sqrt{2 \cdot B_{E\gamma}}}{c} \tag{7}$$

Table 8 Counts of radiative capture lines of nickel and zirconium calculated by means of Eq. (3) and measured counts

	E_γ (keV)	$\sigma^Z_{E\gamma,\mathrm{th}}$(mb)	$\sigma^Z_{E\gamma}$(mb)	$P_{E\gamma}/\varepsilon_{E\gamma}{:}f_{E\gamma}$ ($\times 10^{-8}$) (Count)	
				Measured	Calculated
Nickel					
^{58}Ni	339.4	167 ± 2	0.23 ± 0.04	2.94 ± 0.15	0.24 ± 0.04
	464.9	843 ± 10	1.15 ± 0.20	1.82 ± 0.08	1.18 ± 0.21
	877.9	236 ± 3	0.32 ± 0.06	1.34 ± 0.07	0.33 ± 0.06
	8120.5	133 ± 3	0.18 ± 0.03	0.20 ± 0.06	0.19 ± 0.03
	8533.5	721 ± 13	0.98 ± 0.17	0.80 ± 0.10	1.01 ± 0.18
	8999.4	1490 ± 30	2.04 ± 0.35	1.99 ± 0.13	2.10 ± 0.37
^{60}Ni	282.9	211 ± 3	0.29 ± 0.05	3.18 ± 0.16	0.30 ± 0.05
	7819.5	336 ± 6	0.46 ± 0.05	0.47 ± 0.15	0.47 ± 0.05
^{62}Ni	6837.5	458 ± 8	0.62 ± 0.11	0.56 ± 0.13	0.64 ± 0.11
Zirconium					
^{90}Zr	1205.6	42 ± 5	2.21 ± 0.62	6.49 ± 0.17	0.94 ± 0.26
	1880.4	16 ± 4	0.84 ± 0.30	4.53 ± 0.16	0.36 ± 0.13
	2042.2	32 ± 8	1.68 ± 0.60	2.59 ± 0.10	0.72 ± 0.26
	2557.8	16 ± 4	0.84 ± 0.30	0.30 ± 0.06	0.36 ± 0.13
	2577.3	16 ± 4	0.84 ± 0.30	0.77 ± 0.08	0.36 ± 0.13
^{91}Zr	560.9	28.5 ± 0.5	1.50 ± 0.38	24.6 ± 0.7	0.64 ± 0.16
	934.5	125 ± 5	6.58 ± 1.70	80 ± 2	2.80 ± 0.73
	1405.1	30 ± 1	1.58 ± 0.41	3.76 ± 0.16	0.67 ± 0.17

E_γ is the gamma-ray energy, $P_{E\gamma}/\varepsilon_{E\gamma}{:}f_{E\gamma}$ the net count in the gamma-ray peak divided by the full-energy-peak efficiency and the gamma-ray self-absorption factor, $\sigma^Z_{E\gamma,th}$ is the elemental cross section for production of prompt gamma rays by thermal neutron capture and $\sigma^Z_{E\gamma}$ is the neutron spectrum-averaged cross section for gamma-ray production by epithermal and fission neutron capture obtained by Eq. (5)

with $B_{E\gamma}$ the area of the background below the gamma line of interest and c a predefined value for the relative uncertainty of the peak area.

The DL of nickel and zirconium were determined from their most intense gamma lines at 1453.6 keV (^{58}Ni, $\sigma_{E\gamma}(90°) = 338$ mb) and 933.8 keV (^{92}Zr, $\sigma_{E\gamma}(90°) = 1068$ mb), respectively, for a counting time of 12 h and for c = 0.5 corresponding to a peak area uncertainty of 50%. Here, the value of $B_{E\gamma}$ was extracted from the beam background spectrum measured with the new version of the FaNGaS instrument [3] which delivers a fast neutron flux at sample position of 1.13×10^8 cm^{-2} s^{-1}. In this case, the smallest amounts of nickel and zirconium that can be detected are 0.7 mg and 1.4 mg, respectively.

Conclusions

Prompt gamma rays induced by (n,n′γ)-, (n,pγ)-, (n,npγ)- and (n,γ)-reactions on nickel and by (n,n′γ) and (n,γ) on zirconium were measured with the FaNGaS instrument operated at FRM II and their relative intensities and fission-neutron spectrum-averaged partial production cross sections were determined. In total, 167 prompt gamma lines were observed for nickel. From these, 128 were associated to (n,n′γ) reactions (41 from ^{58}Ni, 48 from ^{60}Ni, 15 from ^{61}Ni, 18 from ^{62}Ni and 6 from ^{64}Ni), 32 to ^{58}Ni(n,p)^{58}Co reaction, 2 to ^{58}Ni(n,n + p)^{57}Co reaction and 5 to (n,γ) reactions (3 from ^{58}Ni, 2 from ^{60}Ni, and 1 from ^{62}Ni). In the case of zirconium, 100 prompt gamma lines were detected, 99 assigned to (n,n′γ) reactions (31 from ^{90}Zr, 17 from ^{91}Zr, 24 from ^{92}Zr, 19 from ^{94}Zr and 8 from ^{96}Zr) and 1 to the ^{90}Zr(n,γ)^{91}Zr reaction. Additionally, delayed

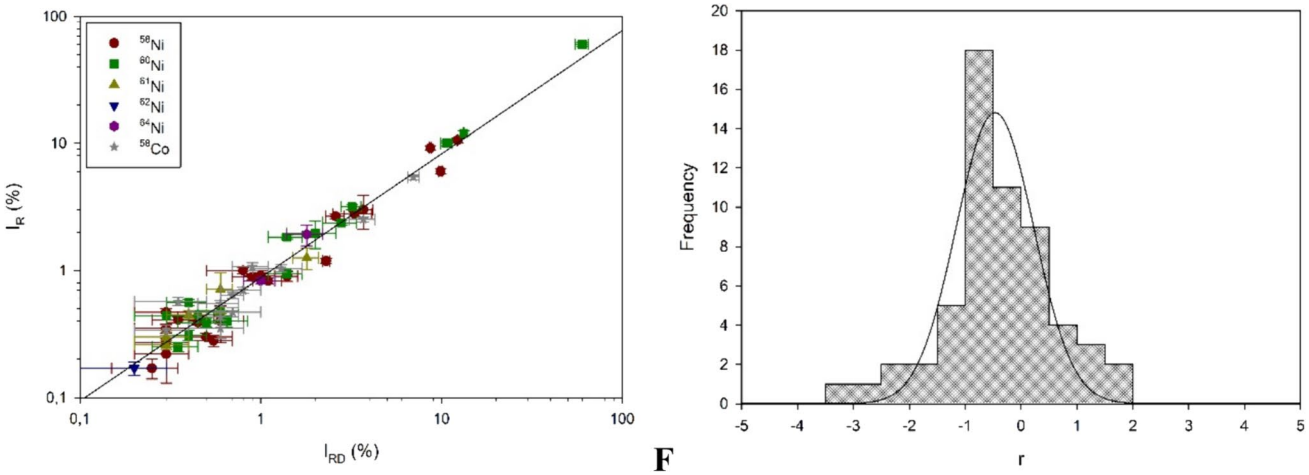

Fig. 7 Comparison of the relative intensities of the prompt gamma rays induced by fast neutrons on nickel obtained in this work with the data tabulated in the Demidov Atlas [9]. Left figure: linear relationship; the solid line represents the fit of the data with Eq. (6). Right figure: histogram of the residuals r in units of standard deviation [σ] calculated with Eq. (7). The values of r are given in column 8 of Tables 2, 3, 4, 5, 6 and 7. The solid line represents the fit of the data with a Gaussian

Table 9 Gamma rays of ^{90}Zr induced by inelastic scattering of fission neutrons

This work				From Demidov Atlas [9]		r
E_γ (keV)	$P_{E\gamma}/\varepsilon_{E\gamma}{:}f_{E\gamma}$ ($\times 10^{-8}$) (Count)	I_R(relative) (%)	$\langle\sigma_{E\gamma}(90°)\rangle$ (mb)	E_γ (keV)	I_{RD}(relative) (%)	
132.33 ± 0.03[e]	0.70 ± 0.08	0.91 ± 0.11	3.2 ± 0.4	–	–	–
328.8 ± 0.3	1.13 ± 0.15	1.46 ± 0.19	5.2 ± 0.8	331.6 ± 0.8	2.0 ± 0.5	− 1.01
419.51 ± 0.01	7.73 ± 0.31	10.04 ± 0.48	36 ± 2	420.0 ± 0.2	12 ± 2	− 0.97
560.31 ± 0.03[a]	24.0 ± 0.7[b]	31 ± 1	32 ± 3[c]	561.49 ± 0.10	40 ± 3	− 2.85
828.0 ± 0.1	0.38 ± 0.04	0.47 ± 0.04	1.6 ± 0.1			
889.92 ± 0.07	5.50 ± 0.20	7.15 ± 0.31	25 ± 1	890.71 ± 0.10	6.6 ± 0.4	1.08
1031.2 ± 0.2	0.25 ± 0.04	0.32 ± 0.05	1.1 ± 0.2	1030.5 ± 0.8	0.40 ± 0.10	− 0.71
1121.36 ± 0.06	1.63 ± 0.41	2.12 ± 0.53	7.5 ± 1.9	1121.9 ± 0.2	1.6 ± 0.2	0.92
1255.4 ± 0.3	0.12 ± 0.03	0.15 ± 0.04	0.55 ± 0.16	–	–	–
1485.7 ± 0.3	0.42 ± 0.05	0.55 ± 0.06	1.9 ± 0.2	1486.8 ± 0.8	0.75 ± 0.15	− 1.24
1559.6 ± 0.1	0.58 ± 0.07	0.75 ± 0.09	2.7 ± 0.3	1560.3 ± 0.8	0.65 ± 0.15	0.57
1584.1 ± 0.2	0.37 ± 0.04	0.48 ± 0.05	1.7 ± 0.2			
1639.9 ± 0.2	0.41 ± 0.12	0.53 ± 0.15	1.9 ± 0.6	1640.4 ± 0.08	0.35 ± 0.10	0.99
1655.9 ± 0.3	0.39 ± 0.06	0.51 ± 0.08	1.8 ± 0.3	1655.6 ± 1.0	0.35 ± 0.10	1.40
1755.0 ± 0.3	0.86 ± 0.08	1.11 ± 0.09	3.9 ± 0.35			
1822.5 ± 0.5	0.37 ± 0.06	0.48 ± 0.07	1.7 ± 0.3	1824.4 ± 0.08	0.65 ± 0.15	− 1.03
1871.12 ± 0.06	0.78 ± 0.04	1.02 ± 0.06	3.6 ± 0.2	1872.1 ± 0.6	1.6 ± 0.3	− 1.89
1913.0 ± 0.3	0.25 ± 0.04	0.32 ± 0.04	1.14 ± 0.18			
1937.0 ± 0.6	0.38 ± 0.05	0.49 ± 0.06	1.75 ± 0.23			
1952.6 ± 0.7	0.43 ± 0.06	0.56 ± 0.07	1.98 ± 0.28			
2013.2 ± 0.7	0.44 ± 0.08	0.57 ± 0.10	2.03 ± 0.36			
2050.3 ± 0.6	0.41 ± 0.06	0.53 ± 0.07	1.89 ± 0.26			
2054.6 ± 0.7	0.28 ± 0.06	0.36 ± 0.07	1.29 ± 0.26			
2185.37 ± 0.04	58 ± 2.0	75 ± 3	268 ± 13	2186.33 ± 0.10	75 ± 2	0
2239.9 ± 0.2	0.49 ± 0.06	0.63 ± 0.07	2.25 ± 0.25			
2280 ± 1	0.20 ± 0.05	0.26 ± 0.06	0.92 ± 0.23			
2269.5 ± 0.8	0.41 ± 0.08	0.53 ± 0.10	1.89 ± 0.36			
2318.45 ± 0.05[e]	15.8 ± 0.5	20.6 ± 0.8	73.0 ± 3.5	2318.92 ± 0.10	20.3 ± 0.8	0.26
2475.1 ± 0.1	0.73 ± 0.05	0.94 ± 0.07	10.1 ± 0.78	2476.3 ± 0.5	0.95 ± 0.20	− 0.05
2747.0 ± 0.1	0.42 ± 0.04	0.54 ± 0.05	1.94 ± 0.19	2748.1 ± 1.0	0.85 ± 0.20	− 1.50
3307.3 ± 0.05	3.65 ± 0.10	4.74 ± 0.18	17 ± 0.8	3308.0 ± 0.8	3.9 ± 0.5	1.58
3841.3 ± 0.5	2.02 ± 0.08	2.60 ± 0.12	9.3 ± 0.5	3841.6 ± 1.0[d]	1.5 ± 0.3	3.40
4228.6 ± 0.6	0.26 ± 0.06	0.33 ± 0.07	1.2 ± 0.3	4227.0 ± 2.0[d]	0.55 ± 0.15	− 1.33

E_γ is the gamma-ray energy, $P_{E\gamma}/\varepsilon_{E\gamma}{:}f_{E\gamma}$ the net count in the gamma-ray peak divided by the full-energy-peak efficiency and the gamma-ray self-absorption factor,I_R the relative intensity of the gamma-ray and $\langle\sigma_{E\gamma}(90°)\rangle$ the fission-neutron spectrum-averaged isotopic cross section for gamma ray production at an angle of 90° between neutron beam and detector determined with Eq. (1). r is the residual calculated by means of Eq. (6)

[a]Contains a contribution of the 561 keV line of ^{92}Zr

[b]Corrected for the contribution of the 561-keV neutron capture line of ^{91}Zr

[c]Calculated with $P_{E\gamma}/\varepsilon_{E\gamma}{:}f_{E\gamma} = (6.9 \pm 0.6)\ 10^8$ obtained using an intensity ratio of 16.4 between 561- and 2747-keV lines of ^{90}Zr [26]

[d]Determined from the double escape peak

[e]Delayed gamma line of ^{90m}Zr

Table 10 Gamma rays of ^{91}Zr induced by inelastic scattering of fission neutrons

This work				From Demidov Atlas [9]		r
E_γ (keV)	$P_{E\gamma}/\varepsilon_{E\gamma}.f_{E\gamma}$ ($\times 10^{-8}$) (Count)	I_R(relative) (%)	$\langle\sigma_{E\gamma}(90°)\rangle$(mb)	E_γ (keV)	I_{RD}(relative) (%)	
150.8 ± 0.1	0.24 ± 0.04	0.31 ± 0.05	5.0 ± 0.8	–	–	–
782.1 ± 0.1	0.76 ± 0.07	0.97 ± 0.09	16 ± 2	783.7 ± 0.8	0.75 ± 0.20	1.00
1068.7 ± 0.3	0.42 ± 0.06	0.54 ± 0.07	8.9 ± 0.9	–	–	–
1151.6 ± 0.2	0.27 ± 0.04	0.39 ± 0.06	5.7 ± 0.8	–	–	–
1204.37 ± 0.08	5.55 ± 0.31[a]	7.21 ± 0.44	117 ± 8	1204.83 ± 0.10	7.0 ± 0.7	0.25
1466.35 ± 0.05	7.99 ± 0.34	10.37 ± 0.51	169 ± 9	1466.23 ± 0.10	11.0 ± 0.8	− 0.66
1619.0 ± 0.5	0.37 ± 0.06	0.48 ± 0.07	7.8 ± 1.3	–	–	–
1881.26 ± 0.04	4.17 ± 0.21[b]	5.41 ± 0.32	88 ± 4	1882.2 ± 0.2	5.5 ± 0.4	− 0.17
2041.63 ± 0.14	1.87 ± 0.27[c]	2.42 ± 0.35	40 ± 6	2042.2 ± 0.3	2.9 ± 0.3	− 1.04
2129.95 ± 0.04	3.86 ± 0.10	5.00 ± 0.18	82 ± 4	2131.16 ± 0.10	5.1 ± 0.5	− 0.19
2168.8 ± 0.2	3.45 ± 0.10	4.48 ± 0.17	73 ± 3	2169.9 ± 0.2	5.0 ± 0.6	− 0.83
2199.2 ± 0.08	1.93 ± 0.08	2.50 ± 0.12	41 ± 2	2200.4 ± 0.8	2.2 ± 0.7	1.44
2365.6 ± 0.2	1.42 ± 0.06	1.84 ± 0.09	30 ± 2	2366.5 ± 0.5	1.9 ± 0.2	− 0.27
2534.3 ± 0.1	0.39 ± 0.07	0.51 ± 0.09	8.3 ± 1.5	2533.5 ± 0.20[d]	1.2 ± 0.3	− 2.20
2577.5 ± 0.6	0.41 ± 0.15[e]	0.53 ± 0.19	3.8 ± 1.4	–	–	–
2693.3 ± 0.4[f]	0.81 ± 0.20	1.05 ± 0.25	7.55 ± 0.3[g]	2694.4 ± 1.0	0.85 ± 0.20	0.62
2774.8 ± 0.5	0.26 ± 0.05	0.33 ± 0.06	5.4 ± 1.0	–	–	–

E_γ is the gamma-ray energy, $P_{E\gamma}/\varepsilon_{E\gamma}.f_{E\gamma}$ the net count in the gamma-ray peak divided by the full-energy-peak efficiency and the gamma-ray self-absorption factor,I_R the relative intensity of the gamma-ray and $\langle\sigma_{E\gamma}\rangle$ the fission-neutron spectrum-averaged isotopic cross section for gamma ray production at an angle of 90° between neutron beam and detector determined with Eq. (1). r is the residual calculated by means of Eq. (6)

[a]Corrected from the contribution of the 1205-keV neutron capture line

[b]Corrected from the contribution of the 1881-keV neutron capture line

[c]Corrected from the contribution of the 2042-keV neutron capture line

[d]Possible interference of the background line of ^{27}Al at 2534-keV

[e]Corrected from the contribution of the 2577-keV neutron capture line

[f]Contains a contribution of the 2694-keV line of ^{92}Zr

[g]Calculated with $P_{E\gamma}/\varepsilon_{E\gamma}.f_{E\gamma} = (0.36 \pm 0.01)\ 10^8$ obtained using an intensity ratio of 0.045 between 2694- and 1466-keV lines of ^{91}Zr [27]

gamma lines of ^{90m}Zr formed by the ^{90}Zr(n,n′)^{90m}Zr reaction were observed. Compared to the work of Demidov et al. [9], 126 gamma lines were detected additionally (78 for nickel and 48 for zirconium). The relative intensities of the lines measured in our work agree reasonably (0.7σ level for nickel, 1.3σ level for zirconium) with the corresponding values given in [9]. For the ^{90}Zr(n,n′)^{90m}Zr reaction we determine an effective cross section of 88 ± 8 mb.

Table 11 Gamma rays of ^{92}Zr induced by inelastic scattering of fission neutrons

This work				From Demidov Atlas [9]		r
E_γ (keV)	$P_{E\gamma}/\varepsilon_{E\gamma}{:}f_{E\gamma}$ ($\times 10^{-8}$) (Count)	I_R(relative) (%)	$\langle\sigma_{E\gamma}(90°)\rangle$(mb)	E_γ (keV)	I_{RD}(relative) (%)	
257.17 ± 0.09	0.46 ± 0.06	0.60 ± 0.08	6.38 ± 0.86	–	–	–
448.8 ± 0.2	6.31 ± 0.29	8.20 ± 0.42	87 ± 5	448.0 ± 0.2	10.2 ± 0.1[a]	−4.63
560.31 ± 0.03	17.7 ± 0.9[b]	23 ± 1	245 ± 15	–	–	–
902.21 ± 0.04	1.99 ± 0.03	2.59 ± 0.07	28 ± 1	–	–	–
912.08 ± 0.03	5.80 ± 0.20	7.53 ± 0.32	80 ± 4	912.6 ± 0.4	6.8 ± 0.1	2.18
933.82 ± 0.03	77 ± 2[c]	100	1068 ± 46	934.55 ± 0.10	100	–
971.7 ± 0.08	0.61 ± 0.10	0.79 ± 0.13	8.5 ± 1.5	971.8 ± 0.8	0.60 ± 0.15	0.06
989.88 ± 0.04	2.54 ± 0.10	3.30 ± 0.17	35 ± 2	990.9 ± 0.3	2.6 ± 0.3	2.03
1131.56 ± 0.03	7.72 ± 0.20	10.00 ± 0.35	107 ± 5	1132.1 ± 0.2	11 ± 2	−0.49
1247.5 ± 0.2	0.33 ± 0.05	0.42 ± 0.06	4.58 ± 0.71	–	–	–
1368.88 ± 0.06	0.92 ± 0.08	1.19 ± 0.10	13 ± 1	1369.1 ± 0.2	0.85 ± 0.15	1.88
1384.9 ± 0.6	0.35 ± 0.06	0.46 ± 0.07	4.9 ± 0.8	–	–	–
1405.11 ± 0.09	3.09 ± 0.21[d]	4.01 ± 0.29	43 ± 3	1405.3 ± 0.3	4.8 ± 0.8	−0.93
1442.7 ± 0.6	0.80 ± 0.10	1.04 ± 0.13	11 ± 1	–	–	–
1675.1 ± 0.1	2.68 ± 0.13	3.48 ± 0.17	37 ± 1	–	–	–
1741.2 ± 0.2	0.40 ± 0.06	0.52 ± 0.08	5.55 ± 0.86	–	–	–
1846.4 ± 0.04	2.84 ± 0.10	3.69 ± 0.15	39 ± 2	1847.0 ± 0.3	4.2 ± 0.4	−1.19
1932.2 ± 0.6	0.43 ± 0.06	0.56 ± 0.07	5.95 ± 0.77	–	–	–
1974.0 ± 0.1	0.85 ± 0.06	1.10 ± 0.08	11.8 ± 0.9	–	–	–
1987.6 ± 0.2	0.39 ± 0.05	0.51 ± 0.06	5.40 ± 0.72	–	–	–
2326.5 ± 0.2	0.39 ± 0.05	0.50 ± 0.06	5.40 ± 0.72	–	–	–
2693.3 ± 0.4	0.45 ± 0.09[e]	0.58 ± 0.11	6.23 ± 1.26	–	–	–
2871.0 ± 0.4	0.23 ± 0.05	0.30 ± 0.06	3.19 ± 0.70	–	–	–
3470.7 ± 0.5	0.31 ± 0.07	0.40 ± 0.12	4.30 ± 0.98	–	–	–

E_γ is the gamma-ray energy, $P_{E\gamma}/\varepsilon_{E\gamma}{:}f_{E\gamma}$ the net count in the gamma-ray peak divided by the full-energy-peak efficiency and the gamma-ray self-absorption factor,I_R the relative intensity of the gamma-ray and $\langle\sigma_{E\gamma}\rangle$ the fission-neutron spectrum-averaged isotopic cross section for gamma ray production at an angle of 90° between neutron beam and detector determined with Eq. (1). r is the residual calculated by means of Eq. (6)

[a]Contains probably interferences of 448-keV (^{176}Hf), 448-keV (^{177}Hf) and 447-keV (^{180}Hf) lines due to hafnium impurity in the sample

[b]Corrected for the contribution of the 561-keV line of ^{90}Zr. See note c in Table 9

[c]Corrected for the contribution of the 934-keV neutron capture line

[d]Corrected from the contribution of the 1405-keV neutron capture line

[e]Corrected from the contribution of the 2694-keV line of ^{91}Zr. See note g in Table 10

Table 12 Gamma rays of ^{94}Zr induced by inelastic scattering of fission neutrons

This work				From Demidov Atlas [9]		r
E_γ (keV)	$P_{E\gamma}/\varepsilon_{E\gamma}{\cdot}f_{E\gamma}$ ($\times 10^{-8}$) (Count)	I_R(relative) (%)	$\langle\sigma_{E\gamma}(90°)\rangle$ (mb)	E_γ (keV)	I_{RD}(relative) (%)	
380.82 ± 0.03	6.93 ± 0.20	9.00 ± 0.34	95 ± 4	381.3 ± 0.3[a]	13.0 ± 0.1	− 11.3
550.05 ± 0.03	10.15 ± 0.30	13.18 ± 0.50	139 ± 6	550.98 ± 0.10	14.1 ± 0.1	− 1.80
751.95 ± 0.04	5.00 ± 0.20	6.49 ± 0.30	68 ± 4	752.70 ± 0.10	6.0 ± 0.5	0.84
918.13 ± 0.03	74 ± 2	96 ± 3	1013 ± 45	918.79 ± 0.10	97 ± 3	− 0.23
1134.99 ± 0.05	1.74 ± 0.08	2.26 ± 0.11	24 ± 1	–	–	–
1138.51 ± 0.03	6.73 ± 0.30	8.74 ± 0.43	92 ± 5	1138.6 ± 0.2	9.6 ± 0.14	− 1.90
1154.7 ± 0.1	0.50 ± 0.06	0.65 ± 0.08	6.8 ± 0.9	–	–	–
1161.1 ± 0.3	0.43 ± 0.06	0.56 ± 0.08	5.9 ± 0.8	–	–	–
1232.03 ± 0.03	4.67 ± 0.20	6.06 ± 0.30	64 ± 3	1232.66 ± 0.10	5.7 ± 0.6	0.54
1390.6 ± 0.1	0.33 ± 0.05	0.43 ± 0.07	4.5 ± 0.7	–	–	–
1410.48 ± 0.04	1.77 ± 0.08	2.30 ± 0.11	24 ± 1	1412.2 ± 0.5	2.4 ± 0.6	− 0.16
1447.1 ± 0.2	0.64 ± 0.07	0.83 ± 0.09	9 ± 1	1448.3 ± 0.8	0.35 ± 0.10	3.57
1588.42 ± 0.08	1.12 ± 0.05	1.45 ± 0.07	24 ± 1	1588.6 ± 0.8	1.9 ± 0.3	− 1.46
1670.78 ± 0.08	7.21 ± 0.20	9.36 ± 0.35	99 ± 4	1671.6 ± 0.3	8.7 ± 0.1	1.43
1778.58 ± 0.06	0.61 ± 0.05	0.79 ± 0.06	8.5 ± 0.7	–	–	–
1928 ± 1	0.26 ± 0.06	0.34 ± 0.07	3.6 ± 0.8	–	–	–
1968.2 ± 0.1	0.65 ± 0.06	0.84 ± 0.08	9 ± 1	–	–	–
2236.5 ± 0.5	0.27 ± 0.04	0.35 ± 0.05	3.7 ± 0.6	–	–	–
2845.2 ± 0.2	0.65 ± 0.07	0.84 ± 0.09	9 ± 1	–	–	–

E_γ is the gamma-ray energy, $P_{E\gamma}/\varepsilon_{E\gamma}{\cdot}f_{E\gamma}$ the net count in the gamma-ray peak divided by the full-energy-peak efficiency and the gamma-ray self-absorption factor,I_R the relative intensity of the gamma-ray and $\langle\sigma_{E\gamma}\rangle$ the fission-neutron spectrum-averaged isotopic cross section for gamma ray production at an angle of 90° between neutron beam and detector determined with Eq. (1). r is the residual calculated by means of Eq. (6)

[a]Contains probably interferences of 380-keV (^{176}Hf) line due to hafnium impurity in the sample

Table 13 Gamma rays of ^{96}Zr induced by inelastic scattering of fission neutrons

This work				From Demidov Atlas [9]		r
E_γ (keV)	$P_{E\gamma}/\varepsilon_{E\gamma}{\cdot}f_{E\gamma}$ ($\times 10^{-8}$) (Count)	I_R(relative) (%)	$\langle\sigma_{E\gamma}(90°)\rangle$(mb)	E_γ (keV)	I_{RD}(relative) (%)	
146.58 ± 0.03	1.94 ± 0.08	2.52 ± 0.12	165 ± 9	146.8 ± 0.2[a]	6.1 ± 0.4	− 8.57
474.78 ± 0.05	0.83 ± 0.21	1.07 ± 0.27	70 ± 18	–	–	–
687.4 ± 0.2	0.74 ± 0.10	0.96 ± 0.13	63 ± 9	–	–	–
770.4 ± 0.6	0.26 ± 0.08	0.34 ± 0.10	22 ± 7	–	–	–
779.2 ± 0.01	0.55 ± 0.06	0.71 ± 0.08	47 ± 5	–	–	–
1018.81 ± 0.1	0.78 ± 0.06	1.01 ± 0.08	66 ± 5	1019.3 ± 0.8	0.90 ± 0.20	0.51
1184.89 ± 0.09	0.37 ± 0.04	0.48 ± 0.05	31 ± 3	–	–	–
1749.65 ± 0.03	5.33 ± 0.20	6.92 ± 0.31	453 ± 23	1750.87 ± 0.10	7.4 ± 0.5	− 0.81

E_γ is the gamma-ray energy, $P_{E\gamma}/\varepsilon_{E\gamma}{\cdot}f_{E\gamma}$ the net count in the gamma-ray peak divided by the full-energy-peak efficiency and the gamma-ray self-absorption factor,I_R the relative intensity of the gamma-ray and $\langle\sigma_{E\gamma}\rangle$ the fission-neutron spectrum-averaged isotopic cross section for gamma ray production at an angle of 90° between neutron beam and detector determined with Eq. (1). r is the residual calculated by means of Eq. (6)

[a]Contains probably interferences of 146-keV (^{179}Hf) line due to hafnium impurity in the sample

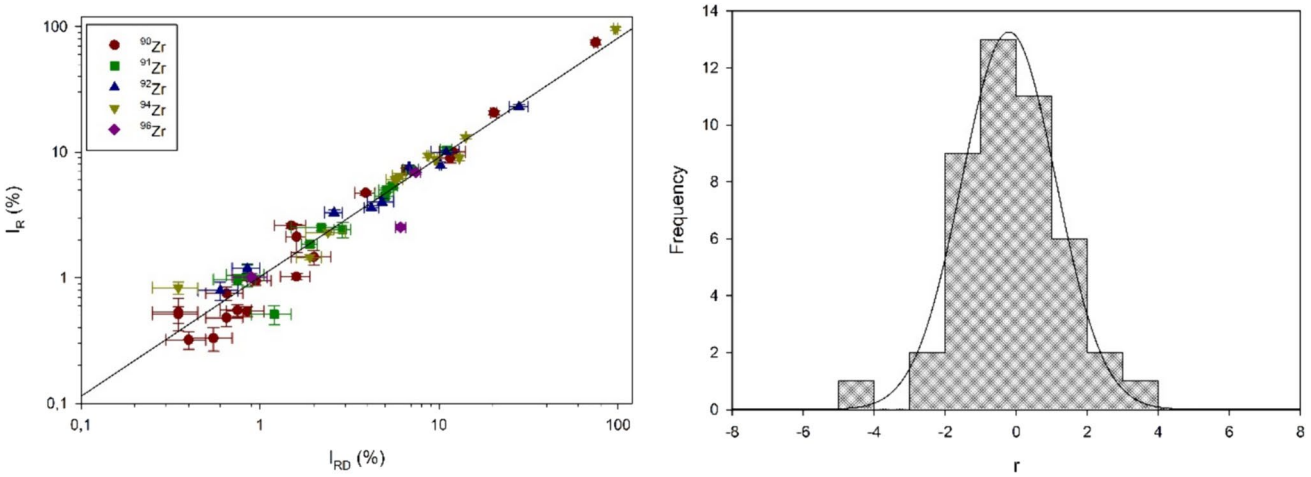

Fig. 8 Comparison of the relative intensities of the prompt gamma rays induced by fast neutrons on zirconium obtained in this work with the data tabulated in the Demidov Atlas [9]. Left figure: linear relationship; the solid line represents the fit of the data with Eq. (6). Right figure: histogram of the residuals r in units of standard deviation [σ] calculated with Eq. (7). The values of r are given in column 8 of Tables 9, 10, 11, 12 and 13. The solid line represents the fit of the data with a Gaussian

The detection limits of nickel and zirconium are 0.7 and 1.4 mg, respectively, for a counting time of 12 h with the actual version of the FaNGaS instrument.

Supplementary Information The online version contains supplementary material available at https://doi.org/10.1007/s10967-024-09570-y.

Funding Open Access funding enabled and organized by Projekt DEAL.

Declarations

Conflict of interest The authors have no competing interests to declare that are relevant to the content of this article. The 5th author, Zsolt Révay is a member of the Editorial Board of the journal. Therefore, he did not take part in the review process in any capacity and the submission was handled by a different member of the editorial board.

References

1. Randriamalala TH, Rossbach M, Mauerhofer E, Révay Zs, Söllrad S, Wagner FM (2016) FaNGaS: a new instrument for (n, n´,γ) reaction measurements at FRM II. Nucl Instrum Meth A806:370–377
2. Ilic Z, Mauerhofer E, Stieghorst C, Revay Zs, Rossbach M, Randriamalala TH, Brückel T (2020) Prompt gamma rays induced by inelastic scattering of fission neutrons on iron. J Radioanal Nucl Chem 325:641–645
3. Ophoven N, Ilic Z, Mauerhofer E, Randriamalala TH, Vezhlev E, Stieghorst C, RévayBrückel ZsT, Jolie J, Strub E (2022) Fast neutron induced gamma rays from (n, n´), (n, p) and (n, α) reactions on CaCO3. J Radioanal Nucl Chem 331:5729–5740
4. Bernstein L, Romano C, Brown D, Casperson R, Descalle MA, Devlin M, Pickett C, Rearden B, Vermeulen C (2019) Final report for the workshop for applied nuclear data activities (WANDA), White Paper LLNL-PROC-769849
5. Mauerhofer E, Ilic Z, Stieghorst C, RévayVezhlev ZsE, Ophoven N, Randriamalala TH, Brückel T (2022) Prompt gamma rays from fast neutron inelastic scattering on aluminum, titanium and copper. J Radioanal Nucl Chem 331:3987–4000
6. Mauerhofer E, Ilic Z, Stieghorst C, RévayRossbach ZsM, Li J, Randriamalala TH, Brückel T (2021) Prompt and delayed gamma rays induced by epithermal and fast neutrons with indium. J Radioanal Nucl Chem 331:535–546
7. Ophoven N, Ilic Z, Mauerhofer E, Randriamalala TH, Vezhlev E, Stieghorst C, RévayBrückel ZsT, Jolie J, Strub E (2023) Prompt gamma rays from fast neutron induced reactions on cerium and chlorine. J Radioanal Nucl Chem 332:3133–3145
8. Ophoven N, Ilic Z, Mauerhofer E, Randriamalala TH, Vezhlev E, Stieghorst C, Révay Zs, Jolie J, Strub E (2024) Prompt gamma rays of terbium induced by inelastic scattering of fission neutrons. J Radioanal Nucl Chem 332:3133–3145
9. Demidov A, Govor L, Cherepantsev M, Ahmed S, Al-Najiar M, Al-Amili N, Al-Assafi N, Rammo N (1978) Atlas of gamma-ray spectra from the inelastic scattering of reactor fast neutrons. Atomizdat, Moscow
10. Breitkreutz H, Wagner FM, Röhrmoser A, Petry W (2008) Spectral fluence rates of the fast reactor neutron beam MEDAPP at FRM II. Nucl Instrum Meth A593:466–471
11. Carlson AD, Pronyaev VG, Capote R, Hale GM, Chen ZP, Duran I, Hambsch FJ, Kunieda S, Mannhart W, Marcinkevicius B, Nelson RO, Neudecker D, Noguere G, Paris M, Simalov SP, Schillebeeckx P, Smith Dl, Tao X, Trkov A, Wallner A, Wang

W (2018) Evaluation of the neutron data standards. Nucl Data Sheets 148:143–188
12. Brown DA et al (2018) ENDF/B-VIII.0: The 8th major release of the nuclear reaction data library with CIELO-project cross sections, new standards and thermal scattering data. Nucl Data Sheets 148:1–142
13. MacFarlane RE, Kahler AC (2010) Methods for processing ENDF/B-VII with NJOY. Nucl Data Sheets 111:2739–2890
14. MacFarlane R, Muir DW, Boicourt RM, Kahler AC, Conlin JL (2017) The NJOY Nuclear data processing system, version 2016. https://doi.org/10.2172/1338791
15. OECD NEA Data Bank, JANIS Book of neutron-induced cross-sections (2020) https://www.oecd-nea.org/janis/book/book-neutron-2020-09.pdf
16. Shibata et al (2011) JENDL-4.0 A new library for nuclear science and engineering. J Nucl Sci Technol 48(1):1–30
17. Nuclear Data Center, Japan atomic energy atomic, tables of nuclear data. https://wwwndc.jaea.go.jp/NuC/index.html
18. Révay Zs, Belgya T, Molnár GL (2005) Application of hypermet-PC in PGAA. J Radioanal Nucl Chem 265:261–265
19. NuDat 3.0 National Nuclear Data Center, Brookhaven National Laboratory. https://www.nndc.bnl.gov/nudat3/
20. Bath MR (1998) Nuclear data sheets for A= 57. Nucl Data Sheets 85:415–536
21. Nesaraja CD, Gereadts SD, Singh B (2010) Nuclear data sheets for A= 58. Nucl Data Sheets 111:897–1092
22. Browne E, Tuli JK (2013) Nuclear data sheets for A= 60. Nucl Data Sheets 114:1849–2022
23. Zuber K, Singh B (2015) Nuclear data sheets for A= 61. Nucl Data Sheets 125:1–200
24. Nichols AL, Singh B, Tuli JK (2012) Nuclear data sheets for A= 61. Nucl Data Sheets 113:973–1114
25. Singh B (2007) Nuclear data sheets for A=64. Nucl Data Sheets 108:197–364
26. Basu SK, Mccutchan EA (2020) Nuclear data sheets for A=90. Nucl Data Sheets 165:1–329
27. Baglin CM (2013) Nuclear data sheets for A=91. Nucl Data Sheets 114:1293–1495
28. Baglin CM (2012) Nuclear data sheets for A=92. Nucl Data Sheets 113:2187–2389
29. Abriola D, Sonzogni AA (2006) Nuclear data sheets for A=94. Nucl Data Sheets 107:2423–2578
30. Abriola D, Sonzogni AA (2008) Nuclear data sheets for A=96. Nucl Data Sheets 109:2501–2655
31. Révay Zs, Firestone RB, Belgya T, Molnár GL (2004) Prompt gamma-ray spectrum catalog. In: Molnár GL (ed) Handbook of prompt gamma activation analysis with neutron beams. Kluwer Academic Publishers, Dordrecht, pp 173–364
32. Tatsuhiko S et al (2018) Features of particle and heavy ion transport code system (PHITS) version 3.02. J Nucl Sci Technol 55:684–769
33. Révay Zs (2009) Determining elemental composition using prompt γ activation analysis. Anal Chem 81:6851–6859